communications biology

A Nature Portfolio journal

Article

https://doi.org/10.1038/s42003-025-07792-8

Theoretical analysis of low-power deep synergistic sono-optogenetic excitation of neurons by co-expressing light-sensitive and mechano-sensitive ion-channels

Sukhdev Roy ✉, Gur Pyari & Himanshu Bansal

The present challenge in neuroscience is to non-invasively exercise low-power and high-fidelity control of neurons situated deep inside the brain. Although, two-photon optogenetic excitation can activate neurons to millimeter depth with sub-cellular specificity and millisecond temporal resolution, it can also cause heating of the targeted tissue. On the other hand, sonogenetics can non-invasively modulate the cellular activity of neurons expressed with mechano-sensitive proteins in deeper areas of the brain with less spatial selectivity. We present a theoretical analysis of a synergistic sono-optogenetic method to overcome these limitations by co-expressing a mechano-sensitive (MscL-I92L) ion-channel with a light-sensitive (CoChR/ChroME2s/ChRmine) ion-channel in hippocampal neurons. It is shown that in the presence of low-amplitude subthreshold ultrasound pulses, the two-photon excitation threshold for neural spiking reduces drastically by 73% with MscL-I92L-CoChR (0.021 mW/μm^2), 66% with MscL-I92L-ChroME2s (0.029 mW/μm^2), and 64% with MscL-I92L-ChRmine (0.013 mW/μm^2) at 5 Hz. It allows deeper excitation of up to 1.2 cm with MscL-I92L-ChRmine combination. The method is useful to design new experiments for low-power deep excitation of neurons and multimodal neuroprosthetic devices and circuits.

Reading and writing neural codes with high spatiotemporal resolution is necessary for understanding neural signal processing in the brain and developing efficient neuroprosthetics[1,2]. Direct brain stimulation and ultrasonic neuromodulation techniques inject direct electric current via electrodes and ultrasound (US) waves, respectively, to modulate neural activity. US waves produce heat or mechanical force that alters the properties of membranes[3,4]. However, the lack of cell-type specificity in these methods restricts their ability to reveal the causal connections between distinct neurons and behavioral processes.

Optogenetics has revolutionized neuroscience research by providing unprecedented spatiotemporal resolution in manipulating and recording neural activity with light with cell-type specificity[5,6]. In optogenetics, light-sensitive proteins are genetically delivered to the desired neural population that enables light to control the electrical activity of these opsin-expressing neurons with sub-cellular spatial and millisecond temporal resolution[7–9].

A major challenge in optogenetics is to achieve low-power, non-invasive, and deep excitation of neurons[10,11]. Light illumination from the tissue surface undergoes significant attenuation due to scattering and absorption, which limits the activable tissue volume[12]. Methods to deliver light to deeply situated neurons involve implantation of optical fiber and micro-sized light-emitting diodes (LED) in the brain tissue, which perturb endogenous neural and glial activity and result in chronic gliosis or permanent damage of the tissue[13]. Additionally, opsins with higher light-sensitivity and red-shifted activation spectrum help in overcoming these limitations, as longer wavelengths can penetrate deeper into the tissue[14–17]. Another key challenge is to achieve temporally precise, high-fidelity, and high-frequency control of activity patterns in targeted neural circuits[8,18–21]. This requires opsins with fast activation and deactivation kinetics to prevent prolonged depolarization or spurious spikes[22,23]. However, the inverse relationship between opsin kinetics and light-sensitivity has been a fundamental bottleneck in simultaneously achieving both low-power as well as fast excitation using optogenetics[24].

To address these challenges, alternative strategies have been developed for deep-brain optogenetic stimulation. One promising approach involves the use of upconversion nanoparticles (UCNPs), which convert near-infrared (NIR) light into visible light, enabling deeper and less invasive

Department of Physics and Computer Science, Dayalbagh Educational Institute, Agra, India. ✉e-mail: sukhdevroy@dei.ac.in

neuronal activation[25]. Molecularly tailored UCNPs can act as optogenetic actuators, stimulating neurons up to 4.5 mm deep transcranial NIR light. The UCNP-mediated approach has been shown to successfully evoke dopamine release in the ventral tegmental area, modulate brain oscillations via medial septal inhibitory neurons, suppress seizures by inhibiting hippocampal excitatory cells, and trigger memory recall. This technique offers a less invasive method for neuronal manipulation and holds promise for remote therapeutic applications[25]. Expanding the potential of nano particles for deep-brain optogenetic stimulation, another innovative approach utilizes NIR illumination to activate macromolecular infrared nanotransducers for deep-brain stimulation-sensitized TRPV1 channels in neurons[26]. This method offers spatially precise control without the need for chronic brain implants or fiber tethering. It enables behavioral modulation in freely moving animals with minimal gliosis and preserves natural behavior. Additionally, pairing this technique with a red-shifted bioluminescent reporter could facilitate an all-optical bidirectional neural interface in behaving animals.

Two-photon (2P) excitation of opsins with high intensity NIR light enables optogenetic stimulation of deeply situated neurons without implanting any light source[27,28]. 2P all-optical physiology opens up tremendous prospects for probing neural codes[28]. However, almost constant single-channel conductance of opsins and limited spot size of light in 2P excitation requires very high-intensity to achieve sufficient photocurrent to generate an action potential (AP), which induces unwanted heating effects in large volume excitation[29].

To address these challenges, there has been a rapid development of new opsins in recent years that offer enhanced control, larger photocurrents, better kinetics, higher photosensitivity, spectral tuning with a broader activation spectrum, improved protein stability along with light-delivery systems[10,11,15,16,30,31]. Blue light-sensitive channelrhodopsin (ChR) variants CoChR and ChroME exhibit enhanced expression, larger photocurrent, and faster kinetics compared to ChR2[8,9,22]. ChRmine, the recently discovered marine opsin, is one of the most promising opsins[14]. It has enabled low-power (0.03 mW/mm^2), deep tissue activation (7 mm), and high-frequency (40–60 Hz) control of various cell types that includes hippocampal neurons, fast-spiking interneurons, retinal ganglion neurons, and cardiac cells[14–16,32–34]. These promising features make it a favorable choice amongst existing opsins for diverse applications[32–34]. More recently, new mutants of ChroME have also been reported[16]. Among these mutants, ChroME2s exhibits the largest maximal photocurrent as well as improved light-sensitivity[16].

Recently, sonogenetics has emerged as a promising alternative to optogenetics, using US to non-invasively stimulate neurons in deep brain regions without the constraints of optical attenuation or scattering[35,36]. US has been safely used in biomedical applications for a long time[35]. Unlike light, US can penetrate deep through bones and soft tissue without significant attenuation or scattering that restrict optogenetic techniques[36]. In sonogenetics, genetically expressed mechano-sensitive channels in the neurons provide spatial resolution in non-invasively stimulating desired neural circuits in deeper brain regions[37]. The large conductance mechano-sensitive ion-channel (MscL) family comprises pore-forming membrane proteins that convert mechanical forces applied to cell membranes to electrophysiological responses. MscLs exhibit high conductance (3 nS), which allows the passage of ions, water, and small protein molecules. Recently, a new mutant, named MscL-I92L, formed by substituting isoleucine at position 92 in the transmembrane (TM2) α-helix with leucine has been reported that exhibits enhanced mechano-sensitivity[38]. This critical residue plays a key role in channel gating, and the substitution likely enhances mechano-sensitivity through interactions between the TM1 and TM2 regions[38]. The study has shown that this mutant precisely excites hippocampal neurons at low-pressure (US 0.25 MPa), which is much lower than the pressure (1 MPa) known to penetrate skull and brain tissue with very little impedance or tissue damage[37–39]. Although sonogenetics is useful for excitation of deeply situated neurons, it has limitations in terms of temporal precision and spiking frequency due to the slow kinetics of existing mechano-sensitive channels[40,41].

Recently, sono-optogenetics, a hybrid method, has also emerged that utilizes nanomaterials to convert US into light[42]. It employs mechanoluminescent nanoparticles as nanoscopic light sources delivered through the bloodstream, to enable millisecond-precision optogenetic neuromodulation. In this technique, focused transcranial- US (FUS) excites mechanoluminescent nanoparticles that have a strong emission at 470 nm for optogenetic neural stimulation of ChR2[42]. Nevertheless, there are certain limitations associated with it that include the possibility of immunological reactions with prolonged usage, inefficiencies in converting US to light, restrictions in precision, and safety issues such as tissue heating or unintended effects.

The potential to further enrich this technique lies in the innovative strategy of co-expressing multiple proteins. In optogenetics, co-expression of excitatory and inhibitory opsins has allowed bidirectional control of neurons by changing the color of light[22,43,44]. Furthermore, co-expression of excitatory ChR and fluorescence proteins has enabled simultaneous all-optical reading and writing of neural codes[31]. A similar approach could be applied by co-expressing light-sensitive and mechano-sensitive ion-channels in the same neuron, enabling synergistic excitation with both light and US. Therefore, US can provide subthreshold activation of neural population in the desired region and can supplement optogenetics. Hence, a synergistic combination of optogenetics and sonogenetics could complement the strengths of both approaches. The term synsonoptogenetics is introduced for synergistic sono-optogenetics to describe the simultaneous effect of both optogenetics and sonogenetics within the same neuron and to distinguish it from the existing sono-optogenetic approach[42]. By utilizing both modalities for simultaneous stimulation, this approach would provide multimodal, low-power, and cell-specific control for deep-brain stimulation, offering a more precise and flexible method for neural modulation.

Recently computational models of optical excitation of neurons and optogenetic-based neural prosthetics have significantly improved our knowledge about underlying mechanisms and helped in optimizing the photostimulation conditions to achieve low-power and high-frequency control of different neurons in the brain, retina, and the human heart[45–47]. Recently, a computational study has shown that the broadband activation of various opsins that include, ChRmine, ReaChR, CatCh, CoChR, and its mutants, enable ultralow irradiance activation of retinal ganglion neurons[45]. A preliminary model for pressure-induced ionic current through mechano-sensitive channels (Piezo 1) has also been reported[48].

To study synsonoptogenetics, an integrated computational framework is required to account for light-induced current in opsins, US-induced current in mechano-sensitive channels, and voltage-gated mechanism of natural ion-channels in neurons. For light-induced current, 2P excitation mechanism is required to be incorporated in the well-established model[49,50] for wide-field excitation of ChRs based on previous studies[51–53]. For US-induced current in mechano-sensitive channels, a well-established 4-state model[48] that describes the gating mechanism for the mechano-sensitive protein Piezo1 in HEK293T cells can be adapted for modeling the current kinetics in MscL-I92L, based on reported electrophysiological measurements[38]. For the hippocampal neurons, the well-established single-compartment Hemond neuron model[54,55] can be used that has been widely employed in several studies to investigate various aspects of neural activity, showing its reliability and utility in understanding the dynamics of hippocampal neurons[56–58]. For an integrated synsonoptogenetic model of excitation of neurons, different mechanisms and their combined effects need to be considered.

Hence, the objective of this paper is to theoretically study the electrophysiological response of hippocampal neurons co-expressed with a mechano-sensitive and a light-sensitive ion-channel under simultaneous stimulation with light and US, and to test whether it can lead to noninvasive deep excitation of neurons. Hence, accurate computational models have been formulated for, (i) 2P optogenetic excitation of CoChR/ChroME2s/ChRmine-expressed hippocampal neurons, (ii) US-activated MscL-I92L-

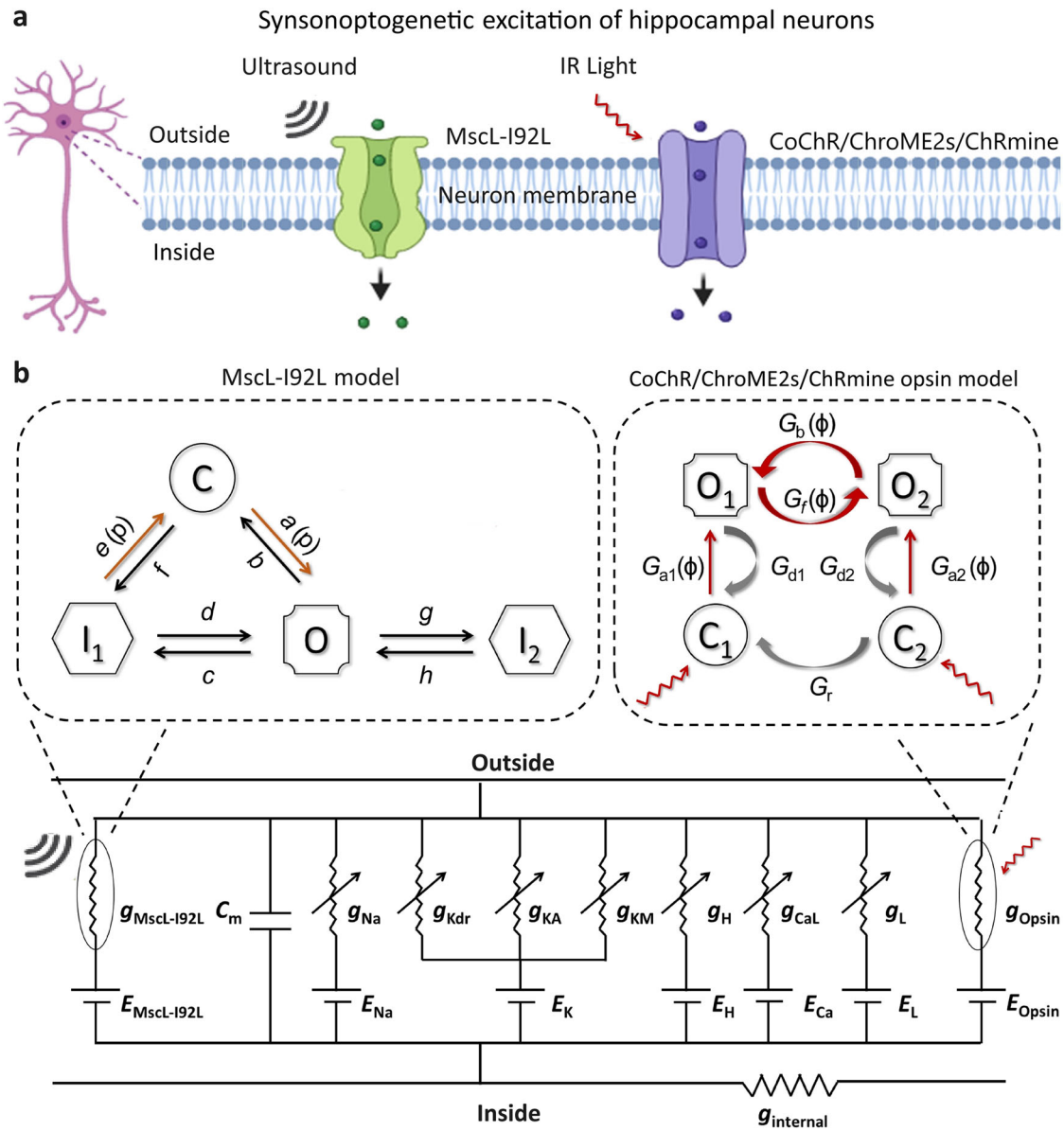

Fig. 1 | Mechanism for synsonoptogenetic excitation of neuron with light and ultrasound. a Schematic of a neuron co-expressed with mechano-sensitive ion-channel (MscL-I92L) and light-sensitive ion-channel (CoChR/ChroME2s/ChRmine opsin). **b** Equivalent circuit diagram that includes currents through different natural- and externally expressed ion-channels across the neuron membrane, with 4-state models for the kinetics of US-induced current through MscL-I92L and IR light-induced current through opsin. Created in BioRender. Pyari, G. (2025) https://BioRender.com/l82k375.

expressed hippocampal neurons, and (iii) synsonoptogenetic excitation of hippocampal neurons co-expressed with CoChR/ChroME2s/ChRmine and MscL-I92L. Further, a detailed analysis has been performed to determine conditions for low-power deep excitation of neurons.

Results

A theoretical framework for analyzing the electrophysiological response of hippocampal neurons co-expressed with mechano-sensitive (MscL-I92L) and light-sensitive (CoChR/ChroME2s/ChRmine) ion-channels under synsonoptogenetic excitation is shown in Fig. 1. The light and US-evoked currents along with natural ionic currents across the neuron membrane and the kinetics of membrane potential have been studied through numerical simulations using Eqs. 1–12 with experimental parameters reported in experiments in Tables 1–4 (Details described in "Methods")[16,38,59,60].

The simulated light-evoked current kinetics in CoChR, ChroME2s, and ChRmine under 2P excitation at 1040 nm are shown in Fig. 2. Among the three opsins, ChRmine exhibits the maximum photocurrent of 3.31 nA on illumination with 1 s light pulse at 1 mW/μm^2 (Fig. 2a). A comparison of the variation in different opsins on illumination with short (10 ms) and long (1 s) light pulses at 1 mW/μm^2 and 1040 nm is shown in Fig. 2b, c. As is evident, the newly discovered ChroME2s exhibits faster turn-off than other ChRs.

Under 2P excitation, the effect of irradiance on light-evoked current in different opsins on illumination with a long (1 s) light pulse at 1040 nm is shown in Fig. 2d–f. It is evident that the change in irradiance not only enhances the light-evoked current amplitude but also speeds up the turn-on kinetics. Also, at higher irradiances, the deactivation rate gets faster in CoChR and ChroME2s at 0.1 and 1 mW/μm^2 as shown in Fig. 2d, e. The corresponding variation of maximum light-evoked current, time to attain maximum light-evoked current (t_{peak}), and the adaptation ratio with irradiance is shown in Fig. 2g–i. The maximum (peak) light-evoked current in CoChR, ChroME2s and ChRmine, saturates at 0.6 mW/μm^2, with a maximum value of 1.25 nA, 1.96 nA and 3.31 nA, respectively (Fig. 2g). At 1 mW/μm^2, the light-evoked current turn-on for CoChR is 15.25 ms, for

Table 1 | Model parameters for ultrasound-evoked current in MscL-I92L[38,48]

Parameter	Value
a_0 (ms^{-1})	0.08
b (ms^{-1})	0.3
c (ms^{-1})	0.018
d (ms^{-1})	0.002
e_0 (ms^{-1})	0.0042
f (ms^{-1})	0
g (ms^{-1})	0.018
h (ms^{-1})	0.1
k (MPa)	6
k_0 (MPa)	7.2
p_0	-57
f_{Hz} (MHz)	29.92
$g_{MscL-I92L}$ (mS/cm^2) in neurons	0.62
$g_{MscL-I92L}$ (nS) for photocurrent	2.9

Table 2 | Model parameters for photo-induced current in CoChR, ChroME2s and ChRmine[14,16,45,59,60]

Parameter	CoChR	ChroME2s	ChRmine
G_{d1}(ms^{-1})	0.06	0.09	0.027
G_{d2}(ms^{-1})	0.015	0.05	0.013
G_r(ms^{-1})	5.7×10^{-5}	5.7×10^{-5}	5.8×10^{-4}
g_{Opsin}(nS) for photocurrent	18.86	37.5	53.26
g_{Opsin}(mS/cm^2) for neurons	0.20	0.41	0.53
ϕ_m(photons mm^{-2} s^{-1})	5×10^{20}	1×10^{21}	0.6×10^{21}
k_1(ms^{-1})	0.2	0.365	0.2
k_2(ms^{-1})	0.1	0.1	0.004
G_{f0}(ms^{-1})	0.0017	0.0006	0.003
G_{b0}(ms^{-1})	0	0.0001	0.01
k_f(ms^{-1})	0.007	0.007	0.001
k_b(ms^{-1})	0.0014	0.0014	0.001
γ	0.12	0.05	0.05
p	1.9	1.8	1.8
q	2	2	2
E_{Opsin} (mV)	25	0	5.64
λ (nm)	1040	1040	1040

ChroME2s is 10.15 ms and for ChRmine is 19.85 ms (Fig. 2h). The adaptation ratio, i.e., the ratio of plateau and peak light-induced current, is a key factor in determining the sustainability of spikes in excitation of neurons. In each opsin it decreases with increase in irradiance, as higher irradiance causes faster desensitization of the light-induced current. The adaptation ratio becomes nearly constant at ~0.3, 0.18, and 0.52 at irradiances above 0.5 $mW/\mu m^2$ for CoChR, ChroME2s, and ChRmine, respectively (Fig. 2i). ChroME2s exhibits a lower adaptation ratio of 0.2 beyond 0.5 $mW/\mu m^2$ due to lower light-induced current plateau (Fig. 2i).

Spike-timing-dependent synaptic plasticity is an important aspect in information processing and in determining a system's switching speed. The light-evoked spiking in different opsin-expressing hippocampal neurons under 2P excitation is shown in Fig. 3. ChRmine-expressing neurons evoke a single AP with latency 21.65 ms, for a 10 ms light pulse at a constant irradiance of 0.04 $mW/\mu m^2$ at 1040 nm (Fig. 3a). The effect of irradiance on AP latency with different opsins-expressing neurons have been shown in Supplementary Fig. 1. The first AP latency on illumination with a 10 ms light pulse at 1040 nm in different opsin-expressing neurons is shown in Fig. 3b. It decreases with increase in irradiance before becoming constant for all opsins. The 2P excitation can trigger AP with a very short 7 ms latency, at 0.5 $mW/\mu m^2$ with ChRmine-expressing neurons (Fig. 3b). The variation of minimum irradiance threshold (MIT) for a single AP with pulse width is shown in Fig. 3c. The MIT for a single AP is 0.55 $mW/\mu m^2$ for a 5 ms light pulse in ChRmine-expressing neurons, which is the minimum among all the three opsins (Fig. 3c).

The generation of temporally precise and high-fidelity optogenetic spiking patterns is essential for encoding information in the spike sequence. The value of minimum irradiance threshold for 100% spiking (MIT_{100}) for different pulse widths of light has also been determined. The spiking response of ChRmine-expressing neurons to 10 ms light pulse at indicated pulse widths and the corresponding MIT_{100} at 10 Hz is shown in Fig. 3d. MIT_{100} decreases with increase in light pulse width. The results show that under 2P excitation, 100% spike fidelity is achieved up to 60 ms light pulse width at 10 Hz, beyond which multiple spikes occur (Fig. 3e). Spiking patterns in different opsin-expressing neurons at different pulse widths and irradiances have been shown in Supplementary Fig. 2. Multiple spikes are elicited only in ChRmine- and CoChR-expressing neurons, when the light pulse width exceeds 60 ms. This is due to slow light-evoked current kinetics of opsins, as it does not allow the membrane potential to return to its resting state between consecutive light pulses. Beyond 60 ms, this cumulative depolarization can result in the emergence of plateau potentials, when the neuron remains in a sustained depolarized state. This plateau further disrupts the membrane's ability to reset, leading to multiple spikes. Supplementary Fig. 2 provides a comparative visualization of these dynamics, highlighting the superior temporally precise spiking with ChroME2s under pulsed stimulation.

Furthermore, the photostimulation conditions for evoking low power high-frequency spiking with single-spike temporal resolution have also been determined. The variation of spiking frequency with stimulation frequency in the three opsin-expressing hippocampal neurons is shown in Fig. 3f. Under optimal illumination condition, ChroME2s-expressing neurons maintain single-spike resolution up to 80 Hz, whereas CoChR-expressing neurons maintain up to 60 Hz. The high-frequency limit of temporally precise spikes in optogenetics is governed by the photocurrent turn-off kinetics[44,61]. As shown in Fig. 2b, c, the photocurrent in ChRmine exhibits slower turn-off kinetics, which may compromise the high-frequency limit. Among the three opsins, although the light power required to evoke spiking with ChRmine is the lowest, it can maintain a single-spike resolution up to 20 Hz as shown in Fig. 3f.

In Fig. 4, the variation of US-evoked current with time in MscL-I92L on illuminating with short (10 ms) and long (1 s) US pulses at different amplitudes and at a fixed frequency of 29.92 MHz is shown. The amplitude of US-evoked current increases with increase in US amplitude and the turn-on kinetics gets faster (Fig. 4a, b). The variation of maximum US-evoked current, time to peak current (t_{peak}), and adaptation ratio with irradiance is shown in Fig. 4c–e. Although MscL-I92L exhibits similar US-evoked current characteristics as in opsins, on increasing irradiance, it shows a higher adaptation ratio > 0.7 throughout the US amplitude range, which highlights its potential for long-term sonogenetic induced neuronal spiking (Fig. 4c, e). The shortest time to maximum US-evoked current is 14.3 ms at a pressure > 0.7 MPa (Fig. 4d).

The US evoked APs in MscL-I92L-expressing hippocampal neurons have been investigated in detail. The effect of US amplitude and pulse width on spike latency is shown in Fig. 5. The variation of membrane potential with time on either stimulating with US pulses of different pulse widths at fixed amplitude 0.45 MPa, or with a fixed 500 ms US pulse at different US amplitudes is shown in Fig. 5a, b. The variation of the number of spikes with US pulse width at different US amplitude values is shown in Fig. 5c. As is evident, the number of spikes increase with US pulse width and saturate after a threshold. Similarly, the number of spikes increase initially and then

Table 3 | Gating function parameters of ion-channels in Hemond neuron circuit model[54,55,76]

I_{ionic}	Gating variable	α	β	x_∞	τ_x (ms)
I_{Na}	$p=3$	$\frac{-0.4(V+6)}{\exp\left[-\left(\frac{V+6}{7.2}\right)\right]-1}$	$\frac{0.124(V+6)}{\exp\left[\frac{V+6}{7.2}\right]-1}$	$\frac{\alpha}{\alpha+\beta}$	$\frac{0.4665}{\alpha+\beta}$
	$q=1$	$\frac{-0.03(V+21)}{\exp\left[-\frac{(V+21)}{1.5}\right]-1}$	$\frac{0.01(V+21)}{\exp\left[\frac{V+21}{1.5}\right]-1}$	$\frac{1}{\exp\left[\frac{V+21}{4}\right]+1}$	$\frac{0.4662}{\alpha+\beta}$
I_{Kdr}	$p=1$	$\exp[-0.113(V-37)]$	$\exp[-0.0791(V-37)]$	$\frac{1}{1+\alpha}$	$\frac{50*\beta}{1+\alpha}$
I_H	$q=1$	$\exp[0.0833(V+75)]$	$\exp[0.0333(V+75)]$	$\frac{1}{\exp\left[\frac{V+73}{8}\right]+1}$	$\frac{\beta}{0.0575(1+\alpha)}$
I_{CaL}	$p=2$	$\frac{15.69\,(-V+81.5)}{\exp\left[\frac{-V+81.5}{10}\right]-1}$	$0.29*\exp\left(-\frac{V}{10.86}\right)$	$\frac{\alpha}{\alpha+\beta}$	$\frac{2*\exp(0.00756(V-4))}{1+\exp(0.0756(V-4))}$
I_{KA}	$p=1$	$\exp\left[-0.0564(V-35)-\frac{0.0376(V-35)}{\exp\left(\frac{V+16}{5}\right)+1}\right]$	$\exp\left[-0.0315(V-35)-\frac{0.021(V-35)}{\left(\exp\left(\frac{(V+16)}{5}\right)+1\right)}\right]$	$\frac{1}{1+\alpha}$	$\frac{3.045*\beta}{1+\beta}$
	$q=1$	$\exp[0.0113(V+32)]$	-	$\frac{1}{1+\alpha}$	$0.26(V+26)$
I_{KM}	$p=1$	$\frac{0.016}{\exp\left[\frac{-(V+52.7)}{23}\right]}$	$\frac{0.016}{\exp\left[\frac{V+52.7}{18.8}\right]}$	$\frac{1}{\exp\left[\frac{-(V+16)}{10}\right]+1}$	$60+\frac{\beta}{0.003(1+\alpha)}$

Table 4 | Hemond neuron model parameters[54,55,76]

Parameter	Value
$g_{Na}(mS/cm^2)$	22
$g_{Kdr}(mS/cm^2)$	10
$g_H(mS/cm^2)$	0.01
$g_{CaL}(mS/cm^2)$	0.01
$g_{KA}(mS/cm^2)$	20
$g_{KM}(mS/cm^2)$	0
$g_L(mS/cm^2)$	0.0394
$E_H(mV)$	−30
$E_{Na}(mV)$	55
$E_K(mV)$	−90
$E_L(mV)$	−64
$\tau_{Ca}(ms)$	100
$I_{DC}(\mu A/cm^2)$	0
$C_m(\mu F/cm^2)$	1.41

saturate beyond a certain US amplitude threshold at different US pulse widths (Fig. 5d).

The results show that to evoke an AP, a minimum US amplitude of 0.29 MPa with a 50 ms pulse width is required. Stimuli beyond this threshold result in APs with shorter latencies (Fig. 5e). The first AP latency in MscL-I92L-expressing neurons at different US amplitudes is shown in Fig. 5f. The shortest latency of 27.5 ms is achieved on stimulating with a 50 ms US pulse at 0.5 MPa (Fig. 5f). Additionally, the variation of the MPT for a single AP with US pulse width is shown in Fig. 5g. The results reveal that initially MIT rapidly decreases with increase in US pulse width and then saturates beyond 100 ms pulse width (Fig. 5g). Hence, the good values of the minimum US pulse width and amplitude to evoke a single AP are 30 ms and 0.35 MPa, respectively (Fig. 5g).

An extensive study of the effect of synsonoptogenetic stimulation with subthreshold US and light pulses on co-expressed MscL-I92L-opsin-expressing hippocampal neurons has also been carried out (Fig. 6). US pulses allow reduction in the irradiance for 2P excitation without altering the spiking fidelity. The AP trace with a fixed light pulse width of 10 ms and an US pulse width of 20 ms at different light irradiances and US amplitudes is shown in Fig. 6. At lower US amplitudes, the ion-channel-expressing neurons are unable to cross the threshold to trigger an AP. However, at 0.02 mW/μm² and 0.4 MPa, an AP is triggered. As the US amplitude increases, the AP is triggered at lower light irradiance levels (Fig. 6a).

The variation in the MIT for a single AP decreases as the US amplitude increases (Fig. 6b). As is evident, MscL-I92L-ChRmine exhibits a lower irradiance threshold for evoking a single AP compared to other opsins. The spiking patterns under light, US, and combined light and US stimulation are shown in Fig. 6c. To determine the MIT_{100}, a 10 ms fixed light pulse at 5 Hz for opsin-expressing neurons and varying US pulse widths at 0.24 MPa and 5 Hz for MscL-I92L-expressing neurons are considered. Figure 6d shows the effect of US pulse width on irradiance threshold for 2P excitation of spikes. It is interesting to observe that 100 ms US pulses at 0.24 MPa enable the light irradiance threshold to decrease from 0.084 mW/μm² to 0.029 mW/μm² in MscL-I92L-ChroME2s (~ 66% decrease), from 0.078 mW/μm² to 0.021 mW/μm² in MscL-I92L-CoChR (~73% decrease), and from 0.038 mW/μm² to 0.013 mW/μm² in MscL-I92L-ChRmine (~64% decrease). At lower US amplitudes, MscL-I92L-expressing neurons achieve maximum depolarization that results in the triggering of APs at a lower irradiance threshold. In addition to offering low power control, this opens up prospects for exploration of deeper brain regions with enhanced spatial resolution.

To understand the mechanism of time delay between light and US stimuli, the effect of the time delay between light and US stimulation is illustrated in Fig. 6e, f. When the light pulse is applied 10 ms before the US pulse, the neurons trigger an AP more quickly compared to when the light pulse is applied 15 ms after the US pulse, even at a low irradiance of 0.028 mW/μm².

The variation in membrane potential and current through both kinds of ion-channels under voltage clamp conditions is shown in Supplementary Fig. 3. As evident, the AP profile differs depending on whether only US is present or only light is present. As light irradiance or US amplitude increases, the number of APs also increase. Additionally, the current during the voltage clamp exhibits different peak amplitudes and distinct turn-on and turn-off profiles.

Further, 0.1 mW/μm² is considered as a safety threshold for light illumination and 100 ms US pulse at 0.24 MPa (Fig. 7a). A good set of photostimulation parameters for which the tissue depth up to which neurons expressed with different MscL-I92L-opsins can be excited have been determined from Fig. 6. The light irradiance reaching up to different depths can be determined using Eq. 13. With simultaneous stimulation of Mscl-I92L-ChRmine-expressing neurons with light (1040 nm) and subthreshold US (29.92 MHz), neurons having an excitation threshold of 0.013 mW/μm², can be excited up to a depth of 1.2 cm, which is an order of magnitude higher depth in comparison to light stimuli alone (Fig. 7b).

The opsin photocurrent is directly proportional to its expression density and thus affects the irradiance threshold for the AP. To study the effect of expression density, the MIT_{100} and MPT_{100} (minimum pressure threshold to evoke 100% spiking) under pulsed illumination have been determined over a wide range of expression densities in MscL-I92L-

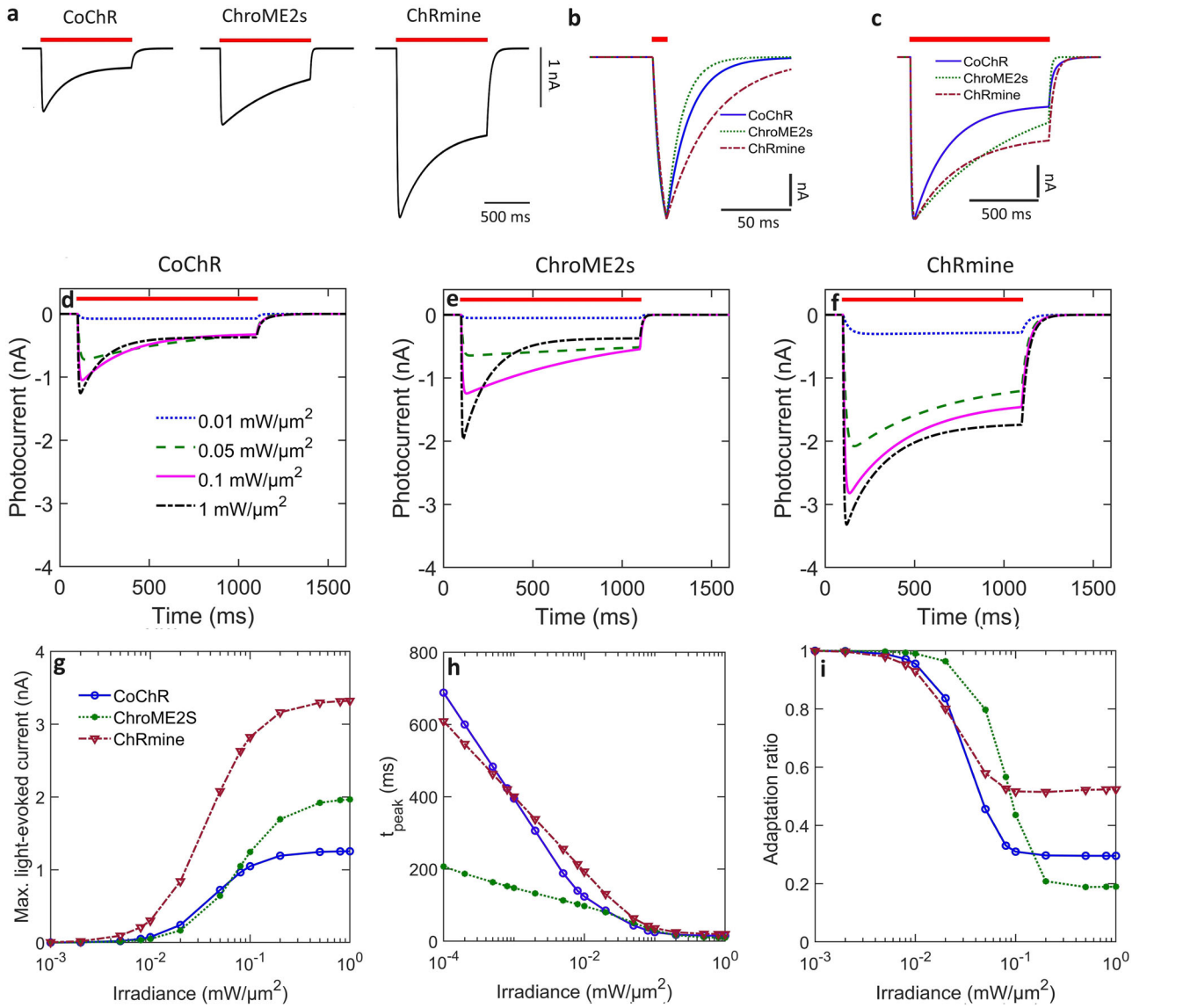

Fig. 2 | Light-evoked current kinetics in CoChR, ChroME2s and ChRmine under two-photon excitation at 1040 nm. a Variation of light-evoked current with time in different opsins with 1 s light pulse at 1 mW/μm^2. Variation of normalized light-evoked current with time on excitation with (**b**) short (10 ms) and (**c**) long (1 s) light pulses at 1 mW/μm^2. Variation of light-evoked current with time in (**d**) CoChR, (**e**) ChroME2s, and (**f**) ChRmine for 1 s light pulse at indicated irradiances, and Corresponding variation of (**g**) maximum light-evoked current amplitude (**h**) time to attain maximum current (t_{peak}), and (**i**) adaptation ratio with irradiance.

ChRmine-expressing neurons. The variation in expression density is considered to be between 0.1 and 10 g, where g is the expression density used in earlier simulations. As is evident, both MIT_{100} and MPT_{100} monotonically decrease with increase in expression density, with the decrease in MPT_{100} being steeper. Hence, expression density can alter the irradiance thresholds as well as the achievable tissue penetration depth (Supplementary Fig. 4).

Discussion

The development of multimodal technologies for non-invasive, spatio-temporally precise neuronal stimulation in the brain and central nervous system has received tremendous attention throughout the previous two decades[1,2]. These technologies are essential for addressing basic neuroscience problems as well as for the diagnosis and treatment of neuropsychiatric illnesses. The integration of neurophysiological and neuroimaging techniques has expanded the understanding of brain functions and disease mechanisms at multiple levels. Optogenetics is capable of excitation, inhibition, and bidirectional control of different neural populations by utilizing the spectral properties and ion-selectivity of different opsins over a wide electromagnetic spectrum[11], whereas sonogenetics primarily enables excitation[37]. However, both techniques cannot individually provide low-power high-frequency deep excitation of neurons. The proposed synsonoptogenetic method not only reduces the irradiance threshold for 2P excitation but also enhances the depth of tissue activation for non-invasive neuronal excitation, marking a milestone in multimodal neurotechnology. The investigation demonstrates how the US pulse width and amplitude are critical in lowering the irradiance threshold for 2P excitation of neurons. A detailed theoretical analysis of the impact of amplitude, pulse width, and pulse frequency of US and NIR light has produced noteworthy results that include changes in adaptation ratio, AP latency, and peak and plateau currents.

2P optogenetic excitation has been shown in various neurons, including ChR2-expressing superior cervical ganglion neurons[53], red-light-activated ChR from Volvox carteri (C1V1) in neocortical brain slices, fast-spiking interneurons, and hippocampal neurons[62–65]. Similar advancements have been shown with ReaChR[52] and Chronos[7]. More recently, 2P holographic photoactivation of ChroME- and CoChR-expressing cortical neurons has achieved optogenetic control of spiking with sub-millisecond temporal precision[7–9]. Beyond excitation, the development of anion-

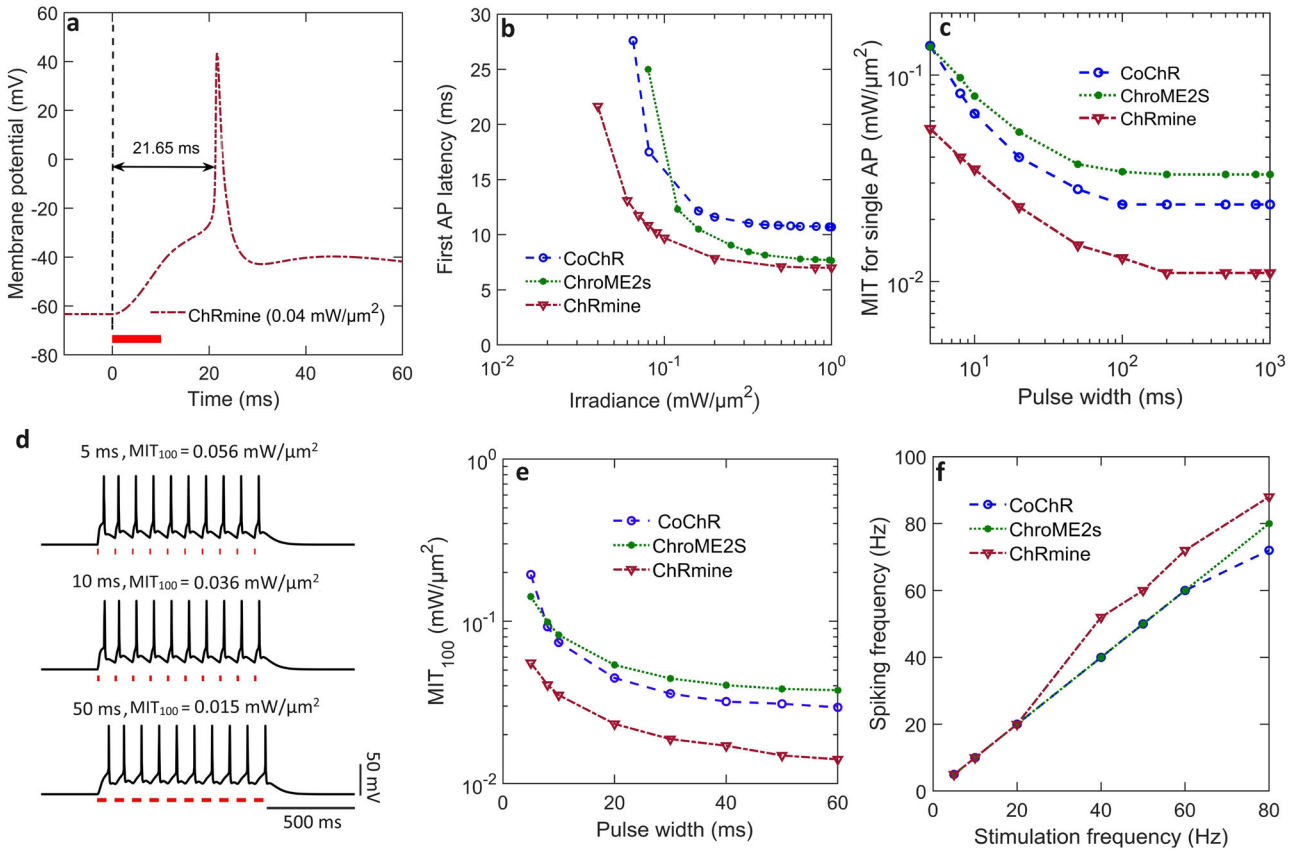

Fig. 3 | Light-evoked spiking in different opsin-expressing hippocampal neurons under two-photon excitation at 1040 nm. a Time variation of membrane potential with 10 ms light pulse at indicated irradiance in ChRmine-expressing neurons. The arrow shows the action potential (AP) latency. **b** Variation of AP latency with light irradiance in different opsin-expressing neurons for 10 ms light pulse. **c** Variation of minimum irradiance threshold (MIT) for single AP with pulse width in different opsin-expressing neurons. **d** Time variation of membrane potential in ChRmine-expressing neurons with 10 light pulses at indicated pulse widths and MIT_{100} (MIT for 100% spiking) at 10 Hz, and (**e**) corresponding variation of MIT_{100} with light pulse width. **f** Variation of spiking frequency with stimulation frequency on stimulation with 10 light pulses each of 5 ms at 0.245 mW/μm² for CoChR, 0.228 mW/μm² for ChroME2s, and 0.059 mW/μm² for ChRmine.

conducting ChRs, such as GtACR2 in cortical interneurons, has enabled 2P holographic suppression at 920 nm with a stimulus power of 30 mW. These channels offer significant advantages over light-driven chloride pumps[60]. Noninvasive excitation of deeply situated neurons in live animal models is important to understand their role in behavioral activities[66,67]. Although, 2P optogenetic excitation is a very precise method to achieve subcellular spatial resolution and sub-millisecond temporal precision, photons at IR wavelength have significant heating effects in the brain tissue[27]. The present synsonoptogenetic method allows excitation of these neurons at lower light irradiances. The low-power excitation of these neurons is also helpful in reaching deeper regions of the brain.

Computational models in optogenetics play a vital role in providing a platform for simulating and understanding the effect of various factors. For optogenetic applications, computational modeling requires a multi-layered approach, ranging from molecular-level models to network-level simulations of opsin-expressing cells. For example, transition rate models of the photocycle of ChR2 and its variants have been reported to simulate photocurrent kinetics[50]. Earlier computational optogenetics research offered profound insights and enabled the optimization of photostimulation conditions for precise neural control[68,69]. It is helpful in simulating contributions of individual ion-channels, change in ion concentrations, and local temperature changes over a wide range of stimulation conditions. Moreover, computational models help in getting insight into the effect of change in expression level of light-sensitive proteins, which is not easily possible through experiment. These models are fundamental for investigating light-induced ionic transport across cell membranes, facilitating the design of experiments, and contributing to the development of innovative treatments for neurological and psychiatric disorders[10,11]. Furthermore, computational approaches assist researchers in engineering new tools and methods for applications within and beyond neuroscience[50,70–73]. Although, efforts to design new opsins with improved conductance and light sensitivity have addressed limitations of earlier mutants in 2P optogenetics, their detailed computational models were missing. The present study provides accurate computational models of 2P optogenetic excitation of neurons with newly engineered opsins, that include ChroME2s and ChRmine[14,16]. These computational models would be useful for detailed analysis and comparison of results over a wide range of photostimulation conditions (Figs. 2 and 3).

The computational models of 2P optogenetic excitation of different opsin, that include CoChR-, ChroME2s-, and ChRmine-expressing hippocampal neurons, have similarly been validated with experimentally reported results[16,59,60]. The variation of photocurrent with time is shown in Supplementary Fig. 5. Upon illumination with a 5 ms light pulse at 10 mW, the maximum photocurrent amplitude is in good agreement with the experimental results reported[16] (Figs. 2E, 1J), showing values of 0.47 nA and 0.7 nA for ChroME2s and ChRmine-expressing neurons, respectively. Furthermore, the variation in photocurrent amplitude with light power is consistent with these reported findings. At a higher light power of 120 mW with a 5 ms pulse, the maximum photocurrent amplitude increases to 1.72 nA in ChroME2s and to 2.35 nA in ChRmine-expressing neurons (Supplementary Fig. 5). The reported experimental high frequency limit for ChroME2s is 40 Hz with 0.57 mW/μm² and for ChRmine is 20 Hz with 0.14 mW/μm² at light pulse of 5 ms[16]. In the present study, the theoretical simulations shown in Fig. 3F, correspondingly match with the high frequency limit for ChroME2s is 40 Hz with 0.228 mW/μm² and for ChRmine

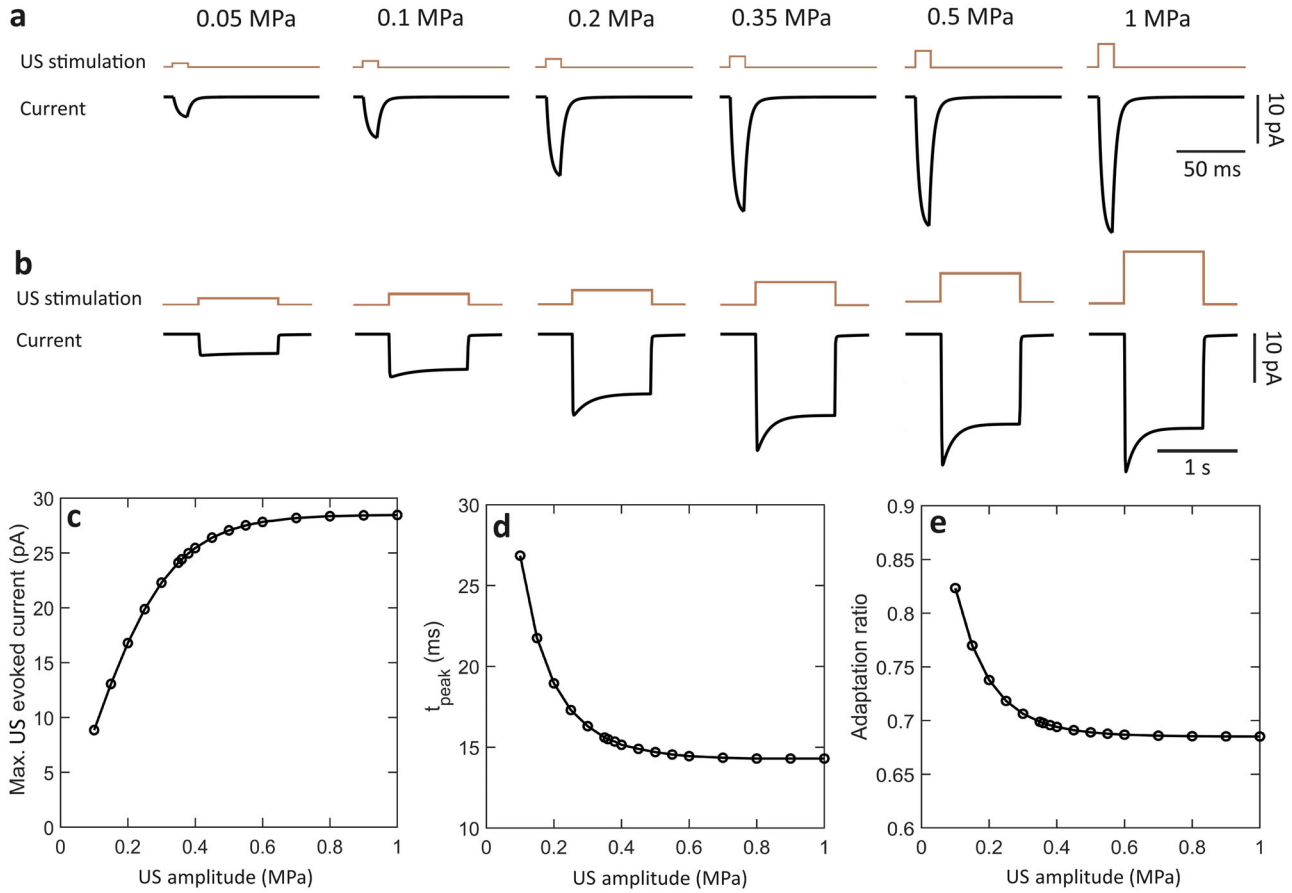

Fig. 4 | US-induced current kinetics in mechano-sensitive ion-channel (MscL-I92L). a, **b** Time variation of US-evoked current on illumination with (upper) short (10 ms), and (lower) long (1 s) US pulses at indicated amplitudes, and corresponding variation of (**c**) maximum US-evoked current, (**d**) t_{peak}, and (**e**) adaptation ratio with US amplitude for 1 s light pulse.

is 20 Hz with 0.059 mW/μm^2 at a light pulse of 5 ms. In the present study, simulations have been carried out at 1040 nm for CoChR due to sufficient experimental data at this wavelength[59]. However, it would be good to compare its performance at its peak absorption wavelength[9].

The study of hippocampal neurons is crucial due to their central role in memory, learning, and neurological disorders such as epilepsy and Alzheimer's disease[74]. The hippocampus features a well-characterized and highly organized circuitry, making it an ideal model for investigating precise neural modulation. Its neurons exhibit distinct excitatory-inhibitory dynamics and play a key role in synaptic plasticity, including long-term potentiation, which underpins learning and memory[75]. However, it is hard for existing precise neuromodulation technologies to excite hippocampus due to its deep location. The proposed synsonoptogenetic excitation method would enable better control of neuronal activity. Recently, a method has been proposed, which involves co-expressing of fast ChRs with step-function opsin to overcome the fundamental limitation of spike failure due to photocurrent desensitization[76]. It has been theoretically shown that ChETA-ChR2(C128A)-expressing hippocampal neurons having an activation threshold of 0.37 mW/mm^2 can be activated up to a depth of 9.1 mm at an extinction coefficient 7.8 cm^{-1}[76]. The proposed synsonoptogenetic method of controlling hippocampal neurons co-expressed with mechano-sensitive and light-sensitive ion-channels with IR light and subthreshold US leads to further enhancement in reaching deeper regions of the brain. The present study shows that MscL-I92L-ChRmine-expressing hippocampal neurons can be safely activated at a depth of 1.2 cm at 0.1 mW/μm^2 and 0.45 MPa (Fig. 7).

In addition to optogenetics, computational sonogenetics offers a approach to studying the mechanisms underlying US-mediated neuromodulation[77]. By modeling how various US pulsing schemes affect ion-channel dynamics and neural firing, this method enables rapid and comprehensive predictions of sonogenetic mediator behavior across diverse ion-channels, cell types, and tissues. These simulations are crucial in optimizing sonogenetic tools for specific cellular and tissue environments and refining US parameters to achieve more selective and precise neural activation. Although, new MscLs have also been discovered to enable precise control of neurons using sonogenetics, their detailed computational models were not reported. The present study provides accurate computational model of sonogenetic excitation of neurons with newly engineered MscL-I92L[38]. This computational model would be useful for detailed analysis of US-induced ionic current and neuron spiking under different ultrasonic illumination conditions (Figs. 2 and 3). To the best of our knowledge, the theoretical model of sonogenetic excitation of hippocampal neurons expressed with MscL-I92L is presented for the first time. The model has been validated by comparing simulated results (Supplementary Fig. 6, 7) with experimentally reported results shown in Fig. 3 of Ye et al.[38]. As it is evident, the variation of AP latency is in good agreement. Notably, increasing the US pressure results in more frequent spikes and a reduced latency for the first spike. According to Ye et al.[38], the first AP latency is 72.3 ± 5.3 ms at 0.25 MPa, and 26.8 ± 4.1 ms at 0.45 MPa. In the present study, the corresponding values are 75 ms at 0.25 MPa and 28 ms at 0.45 MPa, as shown in Supplementary Fig. 7. This computational model would enable detailed analysis and comparison of the response of different neurons under sonogenetic excitation with MscL-I92L.

The US frequency of 29.92 MHz in the present study is the same as used in the experimental study[38]. However, this frequency would experience higher attenuation in the brain. The stimulation protocol used in the present

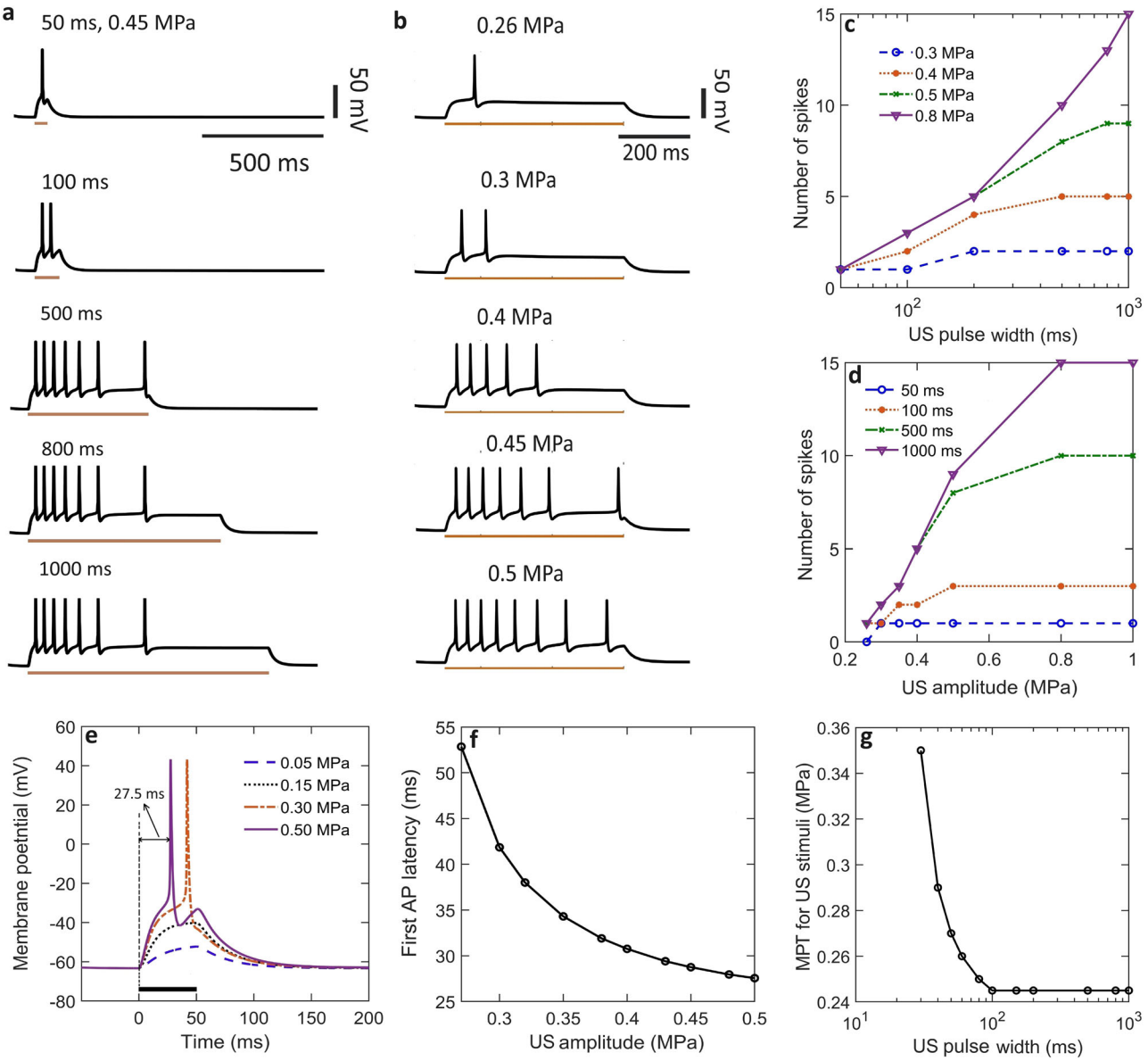

Fig. 5 | Effect of US amplitude and pulse width on spiking in MscL-I92L-expressing hippocampal neurons. Time variation of membrane potential on stimulation with (**a**) US pulses of different pulse widths at 0.45 MPa, and (**b**) 500 ms US pulse at different US amplitudes. Variation of number of spikes with (**c**) US pulse width at different amplitudes and (**d**) US pulse amplitude at different pulse widths. **e** Time variation of membrane potential on stimulation with 50 ms US pulse at indicated US amplitudes. The arrow shows the first action potential (AP) latency at 0.50 MPa. **f** Variation of AP latency with US amplitude for 50 ms US pulse. **g** Variation of minimum pressure threshold (MPT) for US stimuli to evoke an AP with US pulse width.

theoretical simulations is well within the protocols used in the reported experimental studies. For ultrasonic activation, Ye et al.[38] have reported that the peak negative pressure of 0.45 MPa generated a temperature rise of < 0.1°C. On the other hand, the stimulation protocol for 2 P excitation is based on the experimental protocol of Sridharan et al.[16] that claims that there were no unwanted thermal effects. Hence, thermal effects have not been incorporated in the proposed theoretical model. Although including thermal mechanisms in the present model would be important for designing experiments, it would nevertheless increase the complexity of the model.

In sonogenetics, US activates the mechano-sensitive channels by producing mechanical pressure in the neuron membrane. The frequency and amplitude of US are crucial to evoke such a response. Previous research has indicated that focused US can cause neuronal activity by many processes, such as intramembrane cavitation within the bilayer neuron and sonoporation, which is the opening of holes in the lipid bilayer, in addition to activating mechano-sensitive channels[78,79]. While no significant contribution from alternative mechanisms has been observed in the experimental study of sonogenetic excitation of MscL-I92L-expressing neurons under the ultrasonic conditions used[79], it is always possible that these mechanisms could occur and result in a combined effect on neural activity. Integrating all potential processes into the theoretical model of neuronal activation with US would therefore be beneficial. The mechanical index for US stimulations used in the present study ranges from 0.008 to 0.016, which is significantly below the safety threshold of 1.9 for brain tissue[80,81].

In multimodal technologies, alignment of two or more modes of stimulation at a desired location is crucial to optimize the impact. In the present study, 2P excitation and ultrasonic illumination both have been simultaneously used. The light attenuation model used in this study is a simplified approach that considers both absorption and scattering under uniform light illumination on the tissue surface. For US, attenuation has not been simulated as the targeted tissue depth is too shallow for significant US

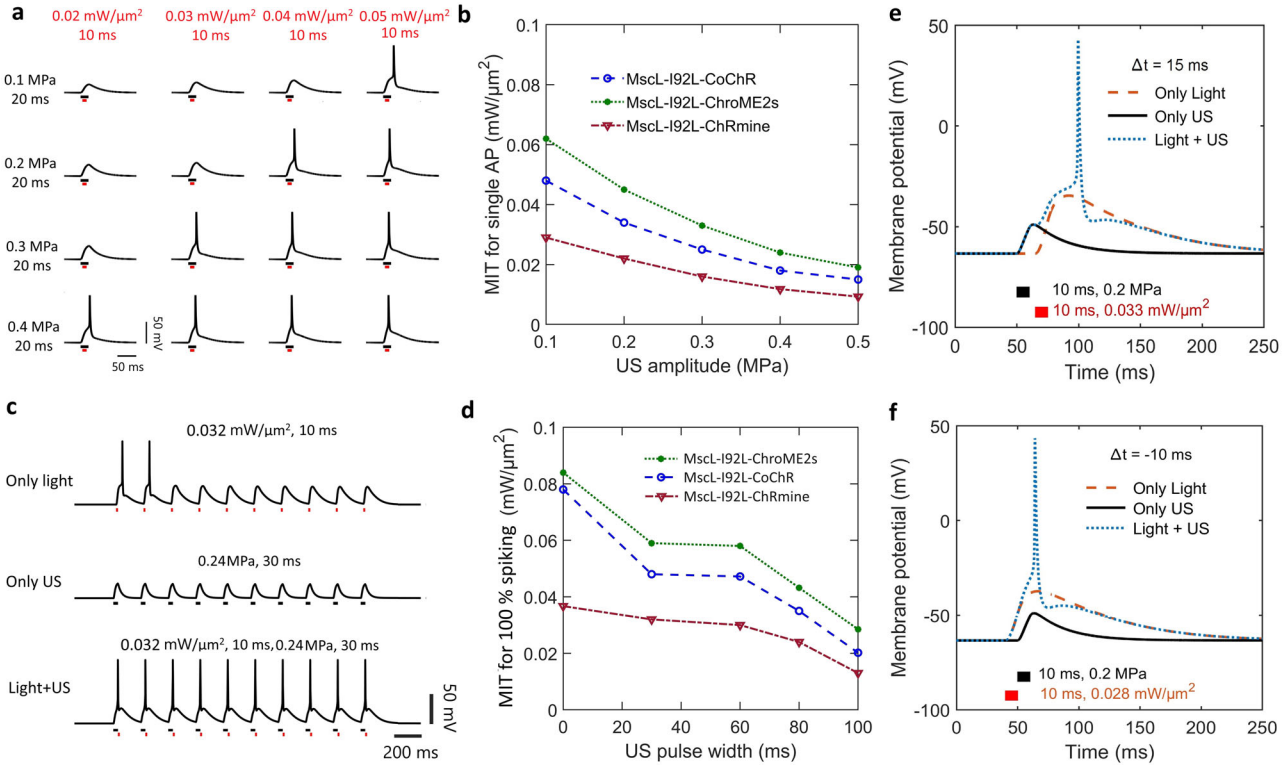

Fig. 6 | Effect of US stimulation on two-photon spiking threshold in hippocampal neurons co-expressed with mechano-sensitive and light-sensitive ion-channels. **a** Effect of the strength of different stimuli. Variation of membrane potential with time on stimulating with both light (10 ms) and US pulse (20 ms) at indicated amplitudes in CoChR-expressing neurons. **b** Variation of MIT for single AP with US amplitude. **c** Spiking pattern at 5 Hz for 10 pulse stimulation with light, with US, and with both light and US. For US pulse widths of 0 ms, 30 ms, and 60 ms, the delay in light stimulation is equal to the US pulse width, and for longer pulse widths (80 ms and 100 ms), the delay in light stimulation is 60 ms. **d** Variation of minimum irradiance threshold for 100% spiking (MIT_{100}) with US pulse width on stimulation with subthreshold US at 0.24 MPa along with 10 light pulses each of 10 ms at 1040 nm, both at 5 Hz. Effect of time delay between light and US stimuli. Variation of membrane potential with time when the light pulse has been applied (**e**) after 15 ms, and (**f**) 10 ms before the US pulse.

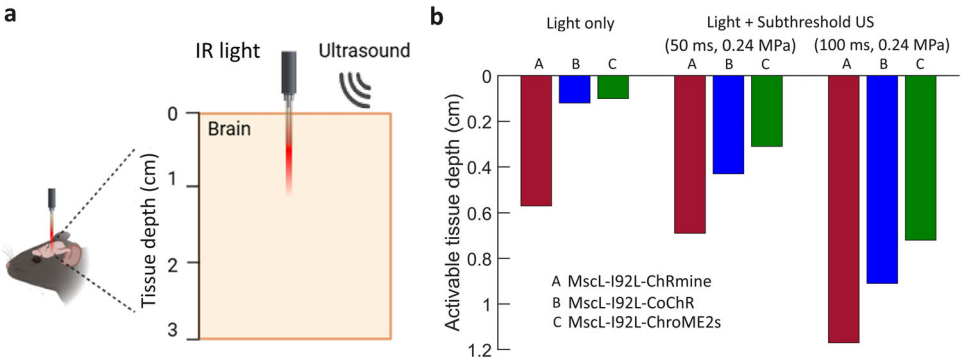

Fig. 7 | Low-power deep excitation of MscL-I92L-ospin-expressing hippocampal neurons on simultaneous two-photon optogenetic and sonogenetic excitations from the surface of the brain tissue. **a** Schematic representation of the mouse brain tissue stimulated with IR light and US. **b** Activable tissue depth of different MscL-I92L-opsin combinations expressing neurons with only IR light, and both IR light and subthreshold US stimulation at 5 Hz. Two-photon excitation on the tissue surface with 10 ms light pulses at 0.1 mW/μm². Created in BioRender. Pyari, G. (2025) https://BioRender.com/i42g023.

attenuation to occur. The light used for 2P excitation is focused to a spot size of approximately 12.5 μm, similar to the dimensions reported in the experimental study[16]. In contrast, the US source is not considered to be focused similar to the experimental conditions reported by Ye et al.[38]. The alignment and positioning of these sources are not challenging, as only the light source requires precise focusing at the desired location, whereas the US source illuminates a broader area.

Furthermore, the ratio of the expression level of MscL and light-sensitive protein molecules would be important to determine the output of applied US and light, respectively. In the present integrated synsonoptogenetic model, the expression level of individual channel has been determined from respective reported experimental results of Sridharan et al.[16] and Ye et al.[38] and the same has been used for simulating results on co-expression. The constant conductance used in the model (0.53 mS/cm² for ChRmine, and 0.62 mS/cm² for MscL-I92L) takes into account for both the respective single channel conductances and expression densities as given in Eqs. 1 and 6. Generally, the single channel conductance for light-sensitive channels (~50–100 fS) is ~6 orders of magnitude smaller than mechano-sensitive channels (~3 nS)[68,82,83]. Different distributions of channels can also be used to directly change the strengths of individual stimulation.

In the present theoretical study, the sonogenetic and optogenetic stimulation have been considered not to affect the kinetics of each other. Experimental studies on co-expression of excitatory and inhibitory opsins and co-expression of multiple opsins have shown that the operations are not

significantly affected[31,84]. However, there can be optical crosstalk due to overlapping of their absorption spectra with excitation wavelength used for bi-directional operation which subsequently leads to undesirable side effects[31,43,44]. In the present study, light-sensitive and mechano-sensitive ion-channels would be activated by light and US, respectively. To the best of our knowledge, there is no experimental evidence to suggest that light influences the kinetics of mechano-sensitive ion-channels or US influences the kinetics of light-sensitive channels, as the mechanisms of light-sensitive and mechano-sensitive ion-channels are distinct. Hence, such interaction has not been considered in the present theoretical model. However, as theoretically shown in Fig. 6, both types of ion-channels, can collectively contribute to neuronal responses when activated synergistically. Furthermore, in optogenetics, ionic-selectivity of light-sensitive channels provides the means to excite or inhibit neuronal activity based on selective ion concentrations across the membrane[6]. This also facilitates the bidirectional control of neuronal activity with different colored lights[31,44]. The MscL-I92L channels are not selective to ions, and thus can only provide excitation at voltage near resting membrane potential[38]. Thus, co-expression of MscL-I92L with an inhibitory opsin would provide potentially crosstalk-free bidirectional control of neurons with both light and US. However, the proposed theoretical prediction needs to be validated through in-vivo experiments.

The potential applications of present study extend to the field of cardiology, where precise control over electromechanical function over a large tissue volume is critical for addressing cardiac disorders as well as to pace the heart. The function of the heart relies on the synchronized activity of electrical and mechanical processes[85]. Disruptions in this synchronization can lead to severe arrhythmias. Optogenetic techniques offer innovative solutions for controlling cardiac activity, particularly defibrillation and cardiac pacing[85,86]. However, implementing light-based interventions in the heart presents significant challenges, including the need for deep tissue penetration and risks associated with light source implantation[17,87,88].

Recent advances in cardiac optogenetics have shown promising results in overcoming these challenges. A recent study in cardiac optogenetics showed that ChRmine can induce contractions in the mouse cardiac cells at extremely low light intensities (~0.1 mW/mm^2)[34]. Optogenetics also enables dynamic and specific modulation of AP duration, which is particularly beneficial for treating conditions like short or long QT syndrome[87,89]. Additionally, computational studies have shown that low-energy defibrillation (~5 $\mu W/mm^2$) in ventricular models is achievable using GtACR1[90]. Recent theoretical advancements with red-shifted opsins, such as ChRmine and bReaChES, can achieve deep tissue excitation (up to ~10 mm) at safe irradiance levels. This capability is critical for terminating re-entry and achieving synchronized cardiac activation[46,91]. A recent computational study demonstrated the effects of light attenuation in different opsins-expressing cardiac cells for effective cardioversion and treatment of tachycardia[91]. The study showed that a five-fold increase in opsin expression levels enhances the tissue suppression depth. Specifically, with ChR2(H134R), the depth increased from 2.24 mm to 3.73 mm, with GtACR1 from 3.78 mm to 5.12 mm, and with ChRmine from 6.63 mm to 9.31 mm[91]. Hence, the proposed synsonoptogenetic method would also be very useful for low-power, deeper excitation or suppression in cardiac optogenetics.

Further, sonogenetics also plays a pivotal role in cardiology. It offers a non-invasive alternative to traditional pacemaker implantation by activating the US-sensitive channel, namely Piezo1, in human cardiomyocytes[81]. This approach enables precise control over cardiac cell activity, allowing for the selective activation or inhibition of cardiomyocytes. Such capability holds significant potential as a defibrillatory mechanism, providing a means to treat severe cardiac arrhythmias[81]. In addition to its potential in arrhythmias, Piezo1 and its gain-of-function mutation (M2241R) are involved in cardiac hypertrophy[92–94]. Regulation of mechano-sensitive ion-channels triggers precise cellular response such as apoptosis which plays a critical role in tumor therapy by eliminating abnormal cells and preventing tumor progression[95]. However, tumor cells resistant to apoptosis often develop therapy resistance, limiting the effectiveness of conventional treatments. Traditional methods such as chemotherapy, radiotherapy, and high-temperature approaches induce apoptosis, but they lack precision, leading to non-specific cell death and significant side effects, including immune suppression, organ damage, and thermal injury to healthy tissues[96]. These limitations underscore the need for more targeted and controlled therapeutic strategies such as sonogenetics. Recently, a promising application of this approach was reported that developed a logic AND-gated nanosystem that employed cationic nanoliposomes to express the MscL-I92L mechano-sensitive ion-channel on tumor cell membranes[97].

Given the unique advantages of sonogenetics, it presents a promising platform for translating remote-control technologies into clinical applications, offering distinct advantages over other techniques. Its applications extend across diverse fields, including neuromodulation, ophthalmology, oncology, stem cell research, and the control of neural reward circuitry[40,41,95,98,99]. Additionally, sonogenetics holds promise for visual restoration and advancing treatments for various nervous system disorders[98,99]. The proposed synsonoptogenetic method will provide synergistic control of cardiac cells using both light and US, offering a approach for achieving low-power and deep-tissue cellular control.

However, despite its many advantages, sonogenetics faces challenges in ensuring specificity, particularly in preventing nonspecific activation of neurons through intrinsic mechano-sensitive ion-channels or peripheral auditory pathways. To minimize these nonspecific effects, recent studies have used short US pulse trains at the lowest effective acoustic pressure[100]. However, the presence of endogenous mechano-sensitive ion-channels might limit the range of usable pressures, emphasizing the need to enhance the sensitivity of sonogenetic mediators and develop strategies for precise in situ monitoring of acoustic pressure. The present study has determined effective photostimulation and US stimulation conditions for low-power and deep control of neural activity (Figs. 3c, d and 5g). The proposed synsonoptogenetic method would also be helpful in enhancing spatial precision in targeting the desired neuron population.

Prior research has shown that transcranial direct current stimulation can enhance the recovery of consciousness in patients with chronic minimally conscious states, and bilateral deep brain electrical stimulation of the central thalamus in disorders of consciousness (DOC) patients can change behavioral responsiveness. However, these technologies are invasive and involve complicated surgery[101]. Intense efforts are focused on improving the spatial resolution and penetration depth of these techniques. Optogenetics has already been widely employed to investigate the causal role of specific neurons or circuits in a variety of behaviors, such as motor control, fear reactions, and decision-making[102,103]. Prior studies have revealed that optogenetic manipulation of neuronal activity in the amygdala using optogenetics can induce or reduce fear responses in animal models[104]. The role of amygdala in modulating fear was confirmed by optogenetic suppression of specific circuits in this brain region, which resulted in a decrease in fear-related behaviors[105]. However, by specifically manipulating neuronal networks thought to be involved in conscious experience, optogenetics also offers a singular chance to investigate the neural correlates of consciousness[106,107]. It gives new insights into the neural mechanisms underlying sleep and anesthesia, two states associated with altered consciousness. Various circuits have been identified for regulating sleep-wake transitions and anesthetic-induced unconsciousness by controlling neurons in the hypothalamus and other brain regions[108]. Several studies have shown effective ultrasonic activation of human cortical, subcortical, and related networks[109–112]. Clinical trials have shown that US can improve specific behavioral outcomes, such as enhanced mood and increased responsiveness in patients with chronic DOC[113,114]. These studies have reported no side effects even with long-term stimulation. The proposed synsonoptogenetic method would provide greater flexibility in controlling specific regions in the brain to study different states of consciousness, recovery of patients from DOC, and behavioral responses.

Limitations

In the present study, a well-established 4-state photocycle model has been adapted to accurately replicate reported experimental findings[49,50,74]. Incorporating more intermediate states in the model could increase the accuracy of the simulations at the expense of increased complexity. Temperature and pH variations that may change in clinical settings have not been incorporated in the present model[29]. Similarly, the light attenuation model assumes uniform illumination on the tissue surface, without considering diffraction and reflection losses[72]. In scenarios involving optical fiber light delivery, the intensity distribution within the tissue depends on factors such as the numerical aperture and core diameter of the fiber[72]. Consequently, neurons at the same depth may receive varying levels of irradiance. To enhance accuracy, these factors should also be incorporated to enable more precise predictions of excitable regions in tissue and organ-scale simulations. The present study also incorporates opsin-specific parameters by fitting the conductance of each opsin to match experimental photocurrent amplitudes. The experimental results of Sridharan et al.[16] were used for opsins ChroME2s and ChRmine, and experimental results of Chen et al.[59] were used for CoChR. The proposed theoretical model is flexible to accommodate variations in opsin conductance. However, the simulations are based on the biophysical properties of healthy mouse tissue, which may differ from those of diseased tissue. Alterations in ion concentrations or ion-channel densities in pathological states could affect irradiance thresholds and frequency responses during optogenetic excitation. These factors also need to be incorporated for further refinement of the models.

The 4-state model of MscL has several limitations. It does not account for unique US-induced mechanical forces, such as cavitation, acoustic streaming, or pressure waves, which may impact gating dynamics differently than static forces[40,41]. Additionally, it neglects lipid-mediated effects, which play a critical role under US-induced membrane deformations. The model also focuses primarily on gating dynamics, overlooking essential aspects such as ion selectivity, conductance, and permeation changes under varying mechanical stimuli key factors for precise sonogenetic neuromodulation. Lastly, US-induced changes in local temperature and viscosity, which can alter MscL behavior, are not incorporated in the model.

In conclusion, an innovative method of low-power deep synsonoptogenetic control of neurons by co-expressing light-sensitive and mechano-sensitive ion-channels has been presented. The proposed method is important as it makes a significant advancement in overcoming a basic challenge in neuroscience by combining the strengths of optogenetics and sonogenetics. Comprehensive theoretical analysis offers valuable insights for designing new experiments involving crosstalk-free bidirectional control, dual-mode regulation of neurons and human ventricular cardiomyocytes, as well as for neural and cardiac prosthesis to enhance recoveries of sensory functions.

Methods

To simulate the activity of hippocampal neurons co-expressed with both light- and mechano-sensitive channels, it is necessary to model the currents that these channels generate in response to stimuli. The natural ion-channels found in hippocampal neurons, when combined with the circuit dynamics of externally produced channels, would thus yield a full circuit for replicating instantaneous voltages in response to various stimuli.

Model for ultrasound-induced current in MscL-I92L

The mechano-sensitive channel (MscL-I92L) from *Escherichia coli* is sensitive to pressure[115]. US waves can produce mechanical pressure over the neuron membrane and activate the MscL-I92L[38]. On activation, it allows ions to flow across the membrane through a non-selective ionic pore.

In general, the US-evoked current in the mechano-sensitive channel ($I_{MscL-I29L}$) can be expressed as,

$$I_{MscL-I29L} = g_{MscL-I92L}\left(V_m - E_{MscL-I92L}\right)S(p,t) \tag{1}$$

where, $g_{MscL-I92L}$ accounts for both the maximum conductance and expression density, V_m is the membrane potential, $E_{MscL-I92L}$ is the reversal potential, and $S(p,t)$ is the US dependent function that explains the likelihood of opening of MscL-I92L molecule due to time-varying US pressure, p is the US pressure wave amplitude, and t is time.

We consider a four-state kinetic model for MscL-I92L to model the channel-opening probability[48]. The model consists of a closed state (C), an open state (O) and two inactivation states (I_1 and I_2). The molecule remains in state C, when there is no pressure, whereas the state O indicates that the channel is in open state, allowing ions to flow across the membrane due to potential gradient. The following set of equations can be used to characterize the transition rates for the kinetics, taking C, O, I_1, and I_2 to represent the fraction of channel molecules in each of the four states at any given moment,

$$\dot{C} = e(p)I_1 + b\,O - \left(f + a(p)\right)C \tag{2}$$

$$\dot{O} = a(p)\,C + d\,I_1 + h\,I_2 - \left(b + c + g\right)O \tag{3}$$

$$\dot{I}_1 = c\,O + f\,C - \left(d + e(p)\right)I_1 \tag{4}$$

$$\dot{I}_2 = g\,O - h\,I_2 \tag{5}$$

where, $C + O + I_1 + I_2 = 1$. $e(p)$ and $a(p)$ are US-dependent transitions from $C \rightarrow O$ and $I_1 \rightarrow C$, defined as $a(p) = a_0\left(1/\left(1+\exp\left(\frac{(p_0 p - k)}{k_0}\right)\right)+1\right) - a_0\left(1/\left(1+\exp\left(\frac{-k}{k_0}\right)\right)+1\right)$ and $e(p) = e_0\left(1/\left(1+\exp\left(\frac{(p_0 p - k)}{k_0}\right)\right)+1\right) - e_0\left(1/\left(1+\exp\left(\frac{-k}{k_0}\right)\right)+1\right)$. MI is also considered for assessing the safety of US stimuli concerning thermal effects. The MI is defined as, MI = $p/\sqrt{f}$, where p is the US amplitude in MPa and f_{Hz} is the ultrasonic frequency in MHz. Simulations in the present study have been carried out at the experimentally reported frequency of 29.92 MHz[38]. Fitting experimental results have established the remaining model parameters (Table 1).

Model for two-photon induced current in CoChR/ChroME2s/ChRmine

On illumination, photoisomerization of the retinal molecule bound with opsin results in opening of ionic pore across the cell membrane due to conformational changes in its structure. Ions pass across the membrane due to the ionic concentration gradient, which alters the neuron membrane potential[6]. The photocurrent that travels across the cell membrane via opsin channels is generally expressed as,

$$I_{Opsin} = g'_{Opsin}(V_m - E_{Opsin}) \tag{6}$$

where, $g'_{Opsin} = g_{Opsin} f(\phi, t)$, with g_{Opsin} as the maximum conductance and $f(\phi,t)$ as a normalized light-dependent function that accounts for the probability of opening of ion-channel. $\phi = \lambda I/hc$, is the photon flux per unit area per unit time, where I is irradiance, λ is wavelength, h is Planck's constant, and c is the speed of light in vacuum[61,72,116–118].

We consider a well-established four-state photocycle model of ChR2 to explain the bi-exponential decay kinetics of photocurrent in CoChR, ChroME2s and ChRmine. The model consists of two closed-states (C_1 and C_2) and two open-states (O_1 and O_2). On illumination with light, the opsin molecule switches from the first closed ground state-C_1 to the open state-O_1. From O_1, the molecule either decays back to C_1 or transits into the second open state-O_2, which is less conductive in comparison to O_1 but has a longer lifetime. The reversible transition between O_1 and O_2 can be both photo and thermal-induced. From C_2, the molecule thermally relaxes to the ground state C_1 or can be photo-excited back to O_2. The transition from C_2 to C_1, also called recovery process of ChRs, is the slowest process in the photocycle.

Experimental results show that ChRmine is the fastest ChR to recover its dark state.

The following set of differential equations can be used to characterize the transition rates of molecules between various states, considering that C_1, O_1, C_2, and O_2 represent the instantaneous proportion of opsin molecules in each of the four states in response to light pulse,

$$\dot{C}_1 = G_{d1}O_1 - G_{a1}C_1 + G_rC_2 \tag{7}$$

$$\dot{O}_1 = G_{a1}C_1 - \left(G_{d1} + G_f\right)O_1 + G_bO_2 \tag{8}$$

$$\dot{O}_2 = G_{a2}C_2 - \left(G_{d2} + G_b\right)O_2 + G_fO_1 \tag{9}$$

$$\dot{C}_2 = G_{a2}O_2 - \left(G_{a2}+G_r\right)C_2 \tag{10}$$

where, $C_1 + O_1 + O_2 + C_2 = 1$. G_{a1} , G_{a2}, G_{d1}, G_{d2}, G_f, G_b and G_r are the rate constants for transitions $C_1 \rightarrow O_1$, $C_2 \rightarrow O_2, O_1 \rightarrow C_1, O_2 \rightarrow C_2, O_1 \rightarrow O_2, O_2 \rightarrow O_1$ and $C_2 \rightarrow C_1$ respectively, defined as $G_{a1}(\varphi) = k_1\varphi^p/(\varphi^p + \varphi_m^p)$, $G_{a2}(\varphi) = k_2\varphi^p/(\varphi^p + \varphi_m^p)$, $G_f(\varphi) = G_{f0} + k_f\varphi^q/(\varphi^q + \varphi_m^q)$, $G_b(\varphi) = G_{b0} + k\varphi^q/(\varphi^q + \varphi_m^q)$. $f(\phi, \quad t) = O_1 + \gamma O_2$ where, γ is the ratio of conductances of states O_1 and O_2. Fitting published experimental results has yielded the model parameters (Table 2).

Integrated model of hippocampal neurons co-expressed with mechano-sensitive and light-sensitive ion-channels

The theoretical model of hippocampal neurons co-expressed with light-sensitive and mechano-sensitive ion-channels can be formulated by integrating I_{Opsin} and $I_{MscL-I92L}$ with the biophysical neuron circuit model (Fig. 1). The rate at which the membrane potential changes in response to light and US can be expressed as,

$$C_m\dot{V} = -I_{ionic} + I_{DC} + I_{Opsin} + I_{MscL-I92L} \tag{11}$$

where, C_m is the membrane capacitance, I_{DC} is the external DC current that controls the excitability of the neuron. I_{ionic} is a sum of ionic currents through naturally occurring voltage-gated ion-channels in the neuron membrane. For hippocampal neurons, each ionic current in I_{ionic} can be expressed as

$$I_{ionic} = (I_{Na} + I_{Kdr} + I_H + I_{CaL} + I_{KA} + I_{KM} + I_L) \tag{12}$$

Each ionic current in I_{ionic} can be expressed as, $I_f = g_fm^ph^q(V - E_f)$, except $I_L = g_L(V - E_L)$, where, g_f is the maximal conductance, m is activation variable (with exponent p), h is inactivation variable (with exponent q), and E_f is the reversal potential of the channel. The rate of change of m and h obey the first-order kinetics according to $\dot{x} = \left(x_\infty - x\right)/\tau_x$. The voltage-dependent functions (x_∞ and τ_x) and values of parameters for hippocampal neuron model are given in Tables 3 and 4, respectively[54,55]. All the simulations have been carried in MATLAB.

Model of light attenuation

Light attenuation due to absorption and scattering by brain tissue can be written as,

$$I(z) = I_0\exp(-z * \delta) \tag{13}$$

where, I_0 is the irradiance from the light source, I is the irradiance reached at cell surface after propagating tissue of thickness z, $\delta = \sqrt{D/\mu_a}$ is the optical penetration depth, and $D = 1/\left(3\left(\mu_a + \mu_s'\right)\right)$ is the diffusivity of light in the medium[12,119,120]. The absorption coefficient (μ_a) and reduced scattering coefficient (μ_s') depend on the wavelength of light and nature of the illuminated tissue. The values of μ_a and μ_s' at 1040 nm are 0.1 cm^{-1} and 10 cm^{-1}, respectively[119].

Reporting summary

Further information on research design is available in the Nature Portfolio Reporting Summary linked to this article.

Data availability

All numerical data used to build figures are available at https://doi.org/10.5281/zenodo.14880424[121].

Code availability

All codes used to build figures are available at https://doi.org/10.5281/zenodo.14880424[121].

Received: 22 September 2024; Accepted: 20 February 2025;
Published online: 06 March 2025

References

1. Polanía, R., Nitsche, M. A. & Ruff, C. C. Studying and modifying brain function with non-invasive brain stimulation. *Nat. Neurosci.* **21**, 174–187 (2018).
2. Bonizzato, M. et al. Multi-pronged neuromodulation intervention engages the residual motor circuitry to facilitate walking in a rat model of spinal cord injury. *Nat. Commun.* **12**, 1–14 (2021).
3. Frey, J. et al. Past, present, and future of deep brain stimulation: hardware, software, imaging, physiology and novel approaches. *Front. Neurol*. **13** (2022).
4. Athanassiadis, A. G. et al. Ultrasound-responsive systems as components for smart materials. *Chem. Rev.* **122**, 5165–5208 (2021).
5. Boyden, E. S., Zhang, F., Bamberg, E., Nagel, G. & Deisseroth, K. Millisecond-timescale, genetically targeted optical control of neural activity. *Nat. Neurosci.* **8**, 1263–1268 (2005).
6. Deisseroth, K. Optogenetics: 10 years of microbial opsins in neuroscience. *Nat. Neurosci.* **18**, 1213–1225 (2015).
7. Ronzitti, E. et al. Recent advances in patterned photostimulation for optogenetics. *J. Opt.* **19**, 113001 (2017).
8. Mardinly, A. R. et al. Precise multimodal optical control of neural ensemble activity. *Nat. Neurosci.* **21**, 881–893 (2018).
9. Shemesh, O. A. et al. Temporally precise single-cell-resolution optogenetics. *Nat. Neurosci.* **20**, 1796–1806 (2017).
10. Bansal, A., Shikha, S. & Zhang, Y. Towards translational optogenetics. *Nat. Biomed. Eng.* **7**, 349–369 (2023).
11. Emiliani, V. et al. Optogenetics for light control of biological systems. *Nat. Rev. Methods Prim.* **2**, 55 (2022).
12. Dufour, S. & De, K. Y. Optrodes for combined optogenetics and electrophysiology in live animals. *Neurophoton*. **2**, 031205 (2015).
13. Guru, A., Post, R. J., Ho, Y. Y. & Warden, M. R. Making sense of optogenetics. *Int. J. Neuropsychopharmacol.* **18**, pyv079 (2015).
14. Marshel, J. H. et al. Cortical layer–specific critical dynamics triggering perception. *Science* **365**, eaaw5202 (2019).
15. Kishi, K. E. et al. Structural basis for channel conduction in the pump-like channelrhodopsin ChRmine. *Cell* **185**, 672–689 (2022).
16. Sridharan, S. et al. High-performance microbial opsins for spatially and temporally precise perturbations of large neuronal networks. *Neuron* **110**, 1139–1155 (2022).
17. Ferenczi, E. A., Tan, X. & Huang, C. L. H. Principles of optogenetic methods and their application to cardiac experimental systems. *Front. Physiol.* **10**, 1096 (2019).
18. Chen, R., Canales, A. & Anikeeva, P. Neural recording and modulation technologies. *Nat. Rev. Mater.* **2**, 16093 (2017).
19. Yun, S. H. & Kwok, S. J. Light in diagnosis, therapy and surgery. *Nat. Biomed. Eng.* **1**, 0008 (2017).
20. Shen, Y., Campbell, R. E., Côté, D. C. & Paquet, M. E. Challenges for therapeutic applications of opsin-based optogenetic tools in humans. *Front. neural circuits* **14**, 542693 (2020).

21. Sahel, J. A. et al. Partial recovery of visual function in a blind patient after optogenetic therapy. *Nat. Med.* **27**, 1223–1229 (2021).
22. Klapoetke, N. C. et al. Independent optical excitation of distinct neural populations. *Nat. Methods* **11**, 338–346 (2014).
23. Mager, T. et al. High frequency neural spiking and auditory signaling by ultrafast red-shifted optogenetics. *Nat. Commun.* **9**, 1750 (2018).
24. Mattis, J. et al. Principles for applying optogenetic tools derived from direct comparative analysis of microbial opsins. *Nat. Methods* **9**, 159–172 (2012).
25. Chen, S. et al. Near-infrared deep brain stimulation via upconversion nanoparticle-mediated optogenetics. *Science* **359**, 679–684 (2018).
26. Wu, X. et al. Tether-free photothermal deep-brain stimulation in freely behaving mice via wide-field illumination in the near-infrared-II window. *Nat. Biomed. Eng.* **6**, 754–770 (2022).
27. Papagiakoumou, E., Ronzitti, E. & Emiliani, V. Scanless two-photon excitation with temporal focusing. *Nat. Methods* **17**, 571–581 (2020).
28. Adesnik, H. & Abdeladim, L. Probing neural codes with two-photon holographic optogenetics. *Nat. Neurosci.* **24**, 1356–1366 (2021).
29. Owen, S. F., Liu, M. H. & Kreitzer, A. C. Thermal constraints on in vivo optogenetic manipulations. *Nat. Neurosci.* **22**, 1061–1065 (2019).
30. Govorunova, E. G. et al. Kalium channelrhodopsins are natural light-gated potassium channels that mediate optogenetic inhibition. *Nat. Neurosci.* **25**, 967–974 (2022).
31. Vierock, J. et al. BiPOLES is an optogenetic tool developed for bidirectional dual-color control of neurons. *Nat. Commun.* **12**, 4527 (2021).
32. Wang, F. et al. Optimization of optogenetic control of Drosophila cardiac function using ChRmine opsin. *Optogenetics Optical Manipulation* **12366**, 33–38 (2023).
33. Alekseev, A. et al. Efficient and sustained optogenetic control of sensory and cardiac systems. *bioRxiv*, 11 (2023).
34. Hsueh, B. et al. Cardiogenic control of affective behavioural state. *Nature* **615**, 292–299 (2023).
35. Gavrilov, L. R., Tsirulnikov, E. M. & Davies, I. A. I. Application of focused ultrasound for the stimulation of neural structures. *Ultrasound Med. Biol.* **22**, 179–192 (1996).
36. Cadoni, S. et al. Ectopic expression of a mechanosensitive channel confers spatiotemporal resolution to ultrasound stimulations of neurons for visual restoration. *Nat. Nanotechnol.* **18**, 667–676 (2023).
37. Ibsen, S., Tong, A., Schutt, C., Esener, S. & Chalasani, S. H. Sonogenetics is a non-invasive approach to activating neurons in Caenorhabditis elegans. *Nat. Commun.* **6**, 1–12 (2015).
38. Ye, J. et al. Ultrasonic control of neural activity through activation of the mechanosensitive channel MscL. *Nano Lett.* **18**, 4148–4155 (2018).
39. Tyler, W. J. Noninvasive neuromodulation with ultrasound? A continuum mechanics hypothesis. *Neuroscientist* **17**, 25–36 (2011).
40. Azadeh, S. S., Lordifard, P., Soheilifar, M. H., Djavid, G. E. & Neghab, H. K. Ultrasound and sonogenetics: a new perspective for controlling cells with sound. *Iran. J. Pharm. Res.* **20**, 151 (2021).
41. Hahmann, J., Ishaqat, A., Lammers, T. & Herrmann, A. Sonogenetics for monitoring and modulating bimolecular function by ultrasound. *Angew. Chem. Int. Ed. Engl.* **63**, e202317112 (2024).
42. Wu, X. et al. Sono-optogenetics facilitated by a circulation-delivered rechargeable light source for minimally invasive optogenetics. *Proc. Natl. Acad. Sci. USA***116**, 26332–26342 (2019).
43. Maimon, B. E., Sparks, K., Srinivasan, S., Zorzos, A. N. & Herr, H. M. Spectrally distinct channelrhodopsins for two-colour optogenetic peripheral nerve stimulation. *Nat. Biomed. Eng.* **2**, 485–496 (2018).
44. Bansal, H., Gupta, N. & Roy, S. Theoretical analysis of low-power bidirectional optogenetic control of high-frequency neural codes with single spike resolution. *Neuroscience* **449**, 165–188 (2020).
45. Bansal, H., Pyari, G. & Roy, S. Theoretical prediction of broadband ambient light optogenetic vision restoration with ChRmine and its mutants. *Sci. Rep.* **14**, 11642 (2024).
46. Pyari, G., Bansal, H. & Roy, S. Ultra-low power deep sustained optogenetic excitation of human ventricular cardiomyocytes with red-shifted opsins: a computational study. *J. Physiol.* **600**, 4653–4676 (2022).
47. Bansal, H., Gupta, N. & Roy, S. Theoretical analysis of optogenetic spiking with ChRmine, bReaChES and CsChrimson-expressing neurons for retinal prostheses. *J. Neural Eng.* **18**, 0460b8 (2021).
48. Lewis, A. H., Cui, A. F., McDonald, M. F. & Grandl, J. Transduction of repetitive mechanical stimuli by Piezo1 and Piezo2 ion channels. *Cell Rep.* **19**, 2572–2585 (2017).
49. Nikolic, K., Jarvis, S., Grossman, N. & Schultz, S. Computational models of optogenetic tools for controlling neural circuits with light.In *Proc. 35th Annual International Conference of the IEEE Engineering in Medicine and Biology Society (EMBC)* 5934–5937, (2013).
50. Nikolic, K. et al. Photocycles of channelrhodopsin-2. *Photochem. Photobiol.* **85**, 400–411 (2009).
51. Picot, A. *2P optogenetics: simulation and modeling for optimized thermal dissipation and current integration* (Doctoral dissertation, Université Sorbonne Paris Cité 2018).
52. Chaigneau, E. et al. Two-photon holographic stimulation of ReaChR. *Front. Cell. Neurosci.* **10**, 234 (2016).
53. Rickgauer, J. P. & Tank, D. W. Two-photon excitation of ChR-2 at saturation. *Proc. Natl. Acad. Sci. USA***106**, 15025–15030 (2009).
54. Alturki, A., Feng, F., Nair, A., Guntu, V. & Nair, S. S. Distinct current modules shape cellular dynamics in model neurons. *Neuroscience* **334**, 309–331 (2016).
55. Hemond, P. et al. Distinct classes of pyramidal cells exhibit mutually exclusive firing patterns in hippocampal area CA3b. *Hippocampus* **18**, 411–424 (2008).
56. Prince, L. Y. et al. Separable actions of acetylcholine and noradrenaline on neuronal ensemble formation in hippocampal CA3 circuits. *PLoS Comput. Biol.* **17**, e1009435 (2021).
57. Roy, R. & Narayanan, R. Ion-channel degeneracy and heterogeneities in the emergence of complex spike bursts in CA3 pyramidal neurons. *J. Physiol.* **601**, 3297–3328 (2023).
58. Zhang, Y. et al. A GPU-based computational framework that bridges neuron simulation and artificial intelligence. *Nat. Commun.* **14**, 5798 (2023).
59. Chen, I. W. et al. In vivo submillisecond two-photon optogenetics with temporally focused patterned light. *J. Neurosci.* **39**, 3484–3497 (2019).
60. Forli, A. et al. Two-photon bidirectional control and imaging of neuronal excitability with high spatial resolution in vivo. *Cell Rep.* **22**, 3087–3098 (2018).
61. Bansal, H., Gupta, N. & Roy, S. Comparison of low-power, high-frequency and temporally precise optogenetic inhibition of spiking in NpHR, eNpHR3. 0 and Jaws-expressing neurons. *Biomed. Phys. Eng. Express* **6**, 045011 (2020).
62. Packer, A. M. et al. Two-photon optogenetics of dendritic spines and neural circuits. *Nat. Methods* **9**, 1202–1205 (2012).
63. Packer, A. M., Russell, L. E., Dalgleish, H. W. & Häusser, M. Simultaneous all-optical manipulation and recording of neural circuit activity with cellular resolution in vivo. *Nat. Methods* **12**, 140–146 (2015).
64. Prakash, R. et al. Two-photon optogenetic toolbox for fast inhibition, excitation and bistable modulation. *Nat. Methods* **9**, 1171–1179 (2012).
65. Rickgauer, J. P., Deisseroth, K. & Tank, D. W. Simultaneous cellular-resolution optical perturbation and imaging of place cell firing fields. *Nat. Neurosci.* **17**, 1816–1824 (2014).

66. Chen, R. et al. Deep brain optogenetics without intracranial surgery. *Nat. Biotechnol.* **39**, 161–164 (2021).
67. Gong, X. et al. An ultra-sensitive step-function opsin for minimally invasive optogenetic stimulation in mice and macaques. *Neuron* **107**, 38–51 (2020).
68. Grossman, N., Nikolic, K., Toumazou, C. & Degenaar, P. Modeling study of the light stimulation of a neuron cell with channelrhodopsin-2 mutants. *IEEE Trans. Biomed. Eng.* **58**, 1742–1751 (2011).
69. Boyle, P. M., Williams, J. C., Ambrosi, C. M., Entcheva, E. & Trayanova, N. A. A comprehensive multiscale framework for simulating optogenetics in the heart. *Nat. Commun.* **4**, 2370 (2013).
70. Foutz, T. J., Arlow, R. L. & McIntyre, C. C. Theoretical principles underlying optical stimulation of a Channelrhodpsin-2 positive pyramidal neuron. *J. Neurophysiol.* **107**, 3235–3245 (2012).
71. Williams, J. C. et al. Computational optogenetics: empirically-derived voltage-and light-sensitive ChR-2 model. *PLoS Comput. Biol.* **9**, 1003220 (2013).
72. Evans, B. D., Jarvis, S., Schultz, S. R. & Nikolic, K. PyRhO: a multiscale optogenetics simulation platform. *Front. Neuroinform.* **10**, 8 (2016).
73. Stefanescu, R. A., Shivakeshavan, R. G., Khargonekar, P. P. & Talathi, S. S. Computational modeling of ChR2 photocurrent characteristics in relation to neural signaling. *Bull. Math. Biol.* **75**, 2208–2240 (2013).
74. Treves, A. & Rolls, E. T. Computational analysis of the role of the hippocampus in memory. *Hippocampus* **4**, 374–391 (1994).
75. Shapiro, M. L. & Eichenbaum, H. Hippocampus as a memory map: synaptic plasticity and memory encoding by hippocampal neurons. *Hippocampus* **9**, 365–384 (1999).
76. Bansal, H., Pyari, G. & Roy, S. Co-expressing fast channelrhodopsin with step-function opsin overcomes spike failure due to photocurrent desensitization in optogenetics: a theoretical study. *J. Neural Eng.* **19**, 026032 (2022).
77. Liu, T. et al. Sonogenetics: recent advances and future directions. *Brain Stimul.* **15**, 1308–1317 (2022).
78. Plaksin, M., Shoham, S. & Kimmel, E. Intramembrane cavitation as a predictive bio-piezoelectric mechanism for ultrasonic brain stimulation. *Phys. Rev. X* **4**, 011004 (2014).
79. Blackmore, J., Shrivastava, S., Sallet, J., Butler, C. R. & Cleveland, R. O. Ultrasound neuromodulation: a review of results, mechanisms and safety. *Ultrasound Med. Biol.* **45**, 1509–1536 (2019).
80. Duck, F. A. Medical and non-medical protection standards for ultrasound and infrasound. *Prog. Biophys. Mol. Biol.* **93**, 176–191 (2007).
81. Li, Y. et al. Sonogenetics is a novel antiarrhythmic mechanism. *Chaos* **35**, 013127 (2025).
82. Lin, J. Y. A user's guide to channelrhodopsin variants: features, limitations and future developments. *Exp. Physiol.* **96**, 19–25 (2011).
83. Song, M., Zhang, M., He, S., Li, L. & Hu, H. Ultrasonic neuromodulation mediated by mechanosensitive ion channels: current and future. *Front. Neurosci.* **17**, 1232308 (2023).
84. Li, L. et al. Colocalized, bidirectional optogenetic modulations in freely behaving mice with a wireless dual-color optoelectronic probe. *Nat. Commun.* **13**, 839 (2022).
85. Entcheva, E. & Kay, M. W. Cardiac optogenetics: a decade of enlightenment. *Nat. Rev. Cardiol.* **18**, 349–367 (2020).
86. Gracheva, E. et al. Dual color optogenetic tool enables heart arrest, bradycardic, and tachycardic pacing in *Drosophila melanogaster*. *Commun. Biol.* **7**, 1056 (2024).
87. Karathanos, T. V., Boyle, P. M. & Trayanova, N. A. Optogenetics-enabled dynamic modulation of action potential duration in atrial tissue: feasibility of a novel therapeutic approach. *Europace* **16**, iv69–iv76 (2014).
88. Bruegmann, T. et al. Optogenetic defibrillation terminates ventricular arrhythmia in mouse hearts and human simulations. *J. Clin. Investig.* **126**, 3894–3904 (2016).
89. Park, S. A., Lee, S. R., Tung, L. & Yue, D. T. Optical mapping of optogenetically shaped cardiac action potentials. *Sci. Rep.* **4**, 6125 (2014).
90. Ochs, A. R., Karathanos, T. V., Trayanova, N. A. & Boyle, P. M. Optogenetic stimulation using anion channelrhodopsin (GtACR1) facilitates termination of reentrant arrhythmias with low light energy requirements: a computational study. *Front. Physiol.* **12**, 718622 (2021).
91. Pyari, G., Bansal, H. & Roy, S. Optogenetically mediated large volume suppression and synchronized excitation of human ventricular cardiomyocytes. *Pflügers Arch. Europ. J. Physiol*. **475**, 1–25 (2023).
92. Bartoli, F. et al. Global PIEZO1 gain-of-function mutation causes cardiac hypertrophy and fibrosis in mice. *Cells* **11**, 1199 (2022).
93. Yu, Z. Y. et al. Piezo1 is the cardiac mechanosensor that initiates the cardiomyocyte hypertrophic response to pressure overload in adult mice. *Nat. Cardiovasc. Res.* **1**, 577–591 (2022).
94. Zhang, Y. et al. Piezo1-mediated mechanotransduction promotes cardiac hypertrophy by impairing calcium homeostasis to activate calpain/calcineurin signaling. *Hypertension* **78**, 647–660 (2021).
95. Zhu, M. et al. Sonogenetics in the treatment of chronic diseases: a new method for cell regulation. *Adv. Sci*. **11**, 2407373 (2024).
96. Hao, Y. et al. Polymeric nanoparticles with ROS-responsive prodrug and platinum nanozyme for enhanced chemophotodynamic therapy of colon cancer. *Adv. Sci.* **7**, 2001853 (2020).
97. Wang, T. et al. A logic and-gated sonogene nanosystem for precisely regulating the apoptosis of tumor Cells. *ACS Appl. Mat. Interfaces* **12**, 56692–56700 (2020).
98. Wu, P. et al. The principles and promising future of sonogenetics for precision medicine. *Theranostics* **14**, 4806 (2024).
99. Tang, J., Feng, M., Wang, D., Zhang, L. & Yang, K. Recent advancement of sonogenetics: a promising noninvasive cellular manipulation by ultrasound. *Genes Dis.* **11**, 101112 (2024).
100. Xian, Q. et al. Modulation of deep neural circuits with sonogenetics. *Proc. Natl. Acad. Sci. USA***120**, e2220575120 (2023).
101. Schiff, N. D. et al. Behavioural improvements with thalamic stimulation after severe traumatic brain injury. *Nature* **448**, 600–603 (2007).
102. Gore, F. et al. Orbitofrontal cortex control of striatum leads economic decision-making. *Nat. Neurosci.* **26**, 1566–1574 (2023).
103. Chen, A. P. et al. Nigrostriatal dopamine modulates the striatal-amygdala pathway in auditory fear conditioning. *Nat. Commun.* **14**, 7231 (2023).
104. Wang, H. et al. A molecularly defined amygdala-independent tetra-synaptic forebrain-to-hindbrain pathway for odor-driven innate fear and anxiety. *Nat. Neurosci.* **27**, 514–526 (2024).
105. Klavir, O., Prigge, M., Sarel, A., Paz, R. & Yizhar, O. Manipulating fear associations via optogenetic modulation of amygdala inputs to prefrontal cortex. *Nat. Neurosci.* **20**, 836–844 (2017).
106. Herrera, C. G. et al. Hypothalamic feedforward inhibition of thalamocortical network controls arousal and consciousness. *Nat. Neurosci.* **19**, 290–298 (2016).
107. Mao, R. et al. Behavioral and cortical arousal from sleep, muscimol-induced coma, and anesthesia by direct optogenetic stimulation of cortical neurons. *Iscience* **27**, 109919 (2024).
108. Sulaman, B. A., Wang, S., Tyan, J. & Eban-Rothschild, A. Neuro-orchestration of sleep and wakefulness. *Nat. Neurosci.* **26**, 196–212 (2023).
109. Chou, T. et al. Transcranial focused ultrasound of the amygdala modulates fear network activation and connectivity. *Brain Stimul.* **17**, 312–320 (2024).

110. Zeng, K. et al. Effects of different sonication parameters of theta burst transcranial ultrasound stimulation on human motor cortex. *Brain Stimul.* **17**, 258–268 (2024).
111. Yaakub, S. N. et al. Transcranial focused ultrasound-mediated neurochemical and functional connectivity changes in deep cortical regions in humans. *Nat. Commun.* **14**, 5318 (2023).
112. Atkinson-Clement, C. et al. Dynamical and individualised approach of transcranial ultrasound neuromodulation effects in non-human primates. *Sci. Rep.* **14**, 11916 (2024).
113. Wan, X., Zhang, Y., Li, Y. & Song, W. An update on noninvasive neuromodulation in the treatment of patients with prolonged disorders of consciousness. *CNS Neurosci. Ther.* **30**, e14757 (2024).
114. Matt, E., Radjenovic, S., Mitterwallner, M. & Beisteiner, R. Current state of clinical ultrasound neuromodulation. *Front. Neurosci.* **18**, 1420255 (2024).
115. Sukharev, S. I., Blount, P., Martinac, B., Blattner, F. R. & Kung, C. A. large-conductance mechanosensitive channel in E. coli encoded by mscL alone. *Nature* **368**, 265–268 (1994).
116. Bansal, H., Pyari, G. & Roy, S. Optogenetic generation of neural firing patterns with temporal shaping of light pulses. *Photonics* **10**, 571 (2023).
117. Gupta, N., Bansal, H. & Roy, S. Theoretical optimization of high-frequency optogenetic spiking of red-shifted very fast-Chrimson-expressing neurons. *Neurophoton* **6**, 025002 (2019).
118. Saran, S., Gupta, N. & Roy, S. Theoretical analysis of low-power fast optogenetic control of firing of Chronos-expressing neurons. *Neurophoton* **5**, 025009 (2018).
119. Gysbrechts, B. et al. Light distribution and thermal effects in the rat brain under optogenetic stimulation. *J. Biophotonics* **9**, 576–585 (2016).
120. Yona, G., Meitav, N., Kahn, I. & Shoham, S. Realistic numerical and analytical modeling of light scattering in brain tissue for optogenetic applications. *eNeuro* **3**, 1 (2016).
121. Roy, S., Pyari, G., & Bansal, H. Theoretical analysis of low-power deep synergistic sono-optogenetic excitation of neurons by co-expressing light-sensitive and mechano-sensitive ion-channels. https://doi.org/10.5281/zenodo.14880424 (2025).

Acknowledgements

The authors are grateful to Revered Professor Prem Saran Satsangi for his kind inspiration and encouragement. They gratefully acknowledge the Department of Science and Technology, India, for the award of a Senior Research Fellowship to G.P. and research grants CRG/2021/005139 and MTR/2021/000742 to S. R.

Author contributions

S.R. and H.B. formulated the problem, G.P. and H.B. carried out the simulations and wrote the original draft. S.R. reviewed the manuscript and G.P. and H.B. edited it.

Competing interests

The authors declare no competing interests.

Additional information

Supplementary information The online version contains supplementary material available at https://doi.org/10.1038/s42003-025-07792-8.

Correspondence and requests for materials should be addressed to Sukhdev Roy.

Peer review information *Communications Biology* thanks the anonymous reviewers for their contribution to the peer review of this work. Primary Handling Editors: Chao Zhou and Benjamin Bessieres. A peer review file is available.